Article

Immunity

Successful Anti-PD-1 Cancer Immunotherapy Requires T Cell-Dendritic Cell Crosstalk Involving the Cytokines IFN-γ and IL-12

Graphical Abstract

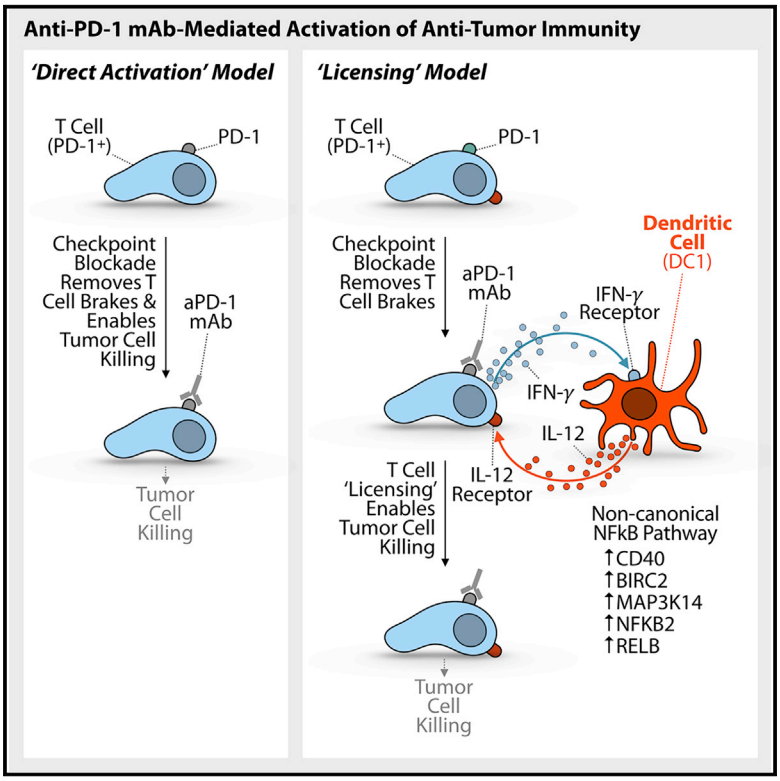

Highlights

- Effective anti-PD-1 anti-tumor responses require IL-12-producing dendritic cells
- Anti-PD-1 indirectly activates IL-12 through IFN-γ produced from CD8$^+$ T cells
- Agonizing the non-canonical NF-κB pathway enhances dendritic cell IL-12 production
- Combining aPD-1 with non-canonical NF-κB agonism enhances checkpoint immunotherapy

Authors

Christopher S. Garris, Sean P. Arlauckas, Rainer H. Kohler, ..., Alfred Zippelius, Ralph Weissleder, Mikael J. Pittet

Correspondence

mpittet@mgh.harvard.edu

In Brief

Anti-PD-1 mAbs can induce sustained clinical responses in cancer but how they function *in vivo* remains incompletely understood. Garris et al. show that effective anti-PD-1 immunotherapy requires intratumoral dendritic cells (DCs) producing IL-12. Anti-PD-1 indirectly activates DCs through IFN-γ released from drug-activated T cells. Furthermore, agonizing the non-canonical NF-κB pathway activates DCs and enhances aPD-1 therapy in an IL-12-dependent manner.

Garris et al., 2018, Immunity *49*, 1148–1161
December 18, 2018
https://doi.org/10.1016/j.immuni.2018.09.024

CellPress

CellPress

Immunity
Article

Successful Anti-PD-1 Cancer Immunotherapy Requires T Cell-Dendritic Cell Crosstalk Involving the Cytokines IFN-γ and IL-12

Christopher S. Garris,[1,2,12] Sean P. Arlauckas,[1,3,12] Rainer H. Kohler,[1] Marcel P. Trefny,[4,5] Seth Garren,[1] Cécile Piot,[1] Camilla Engblom,[1] Christina Pfirschke,[1] Marie Siwicki,[1,2] Jeremy Gungabeesoon,[1] Gordon J. Freeman,[6] Sarah E. Warren,[7] SuFey Ong,[7] Erica Browning,[8] Christopher G. Twitty,[8] Robert H. Pierce,[8] Mai H. Le,[8] Alain P. Algazi,[9] Adil I. Daud,[9] Sara I. Pai,[10] Alfred Zippelius,[4] Ralph Weissleder,[1,3,11] and Mikael J. Pittet[1,3,13,*]

[1]Center for Systems Biology, Massachusetts General Hospital, 185 Cambridge St, CPZN 5206, Boston, MA 02114, USA
[2]Graduate Program in Immunology, Harvard Medical School, Boston, MA 02115, USA
[3]Department of Radiology, Massachusetts General Hospital, 185 Cambridge St, CPZN 5206, Boston, MA 02114, USA
[4]Medical Oncology, Universitätsspital Basel, Basel, Switzerland
[5]Cancer Immunology, Department of Biomedicine and Medical Oncology, University Hospital Basel, Switzerland
[6]Department of Medical Oncology, Dana-Farber Cancer Institute, Harvard Medical School, Boston, MA 02115, USA
[7]NanoString Technologies, 500 Fairview Ave N, Seattle, WA 98109, USA
[8]Oncosec Inc, 5820 Nancy Ridge Drive, San Diego, CA 92121, USA
[9]University of California, San Francisco Medical Center-Mt. Zion, 1600 Divisadero St, San Francisco, CA 94115, USA
[10]Department of Surgery, Massachusetts General Hospital, Harvard Medical School, Boston, MA 02115, USA
[11]Department of Systems Biology, Harvard Medical School, 200 Longwood Ave, Boston, MA 02115, USA
[12]These authors contributed equally to this work
[13]Lead Contact
*Correspondence: mpittet@mgh.harvard.edu
https://doi.org/10.1016/j.immuni.2018.09.024

SUMMARY

Anti-PD-1 immune checkpoint blockers can induce sustained clinical responses in cancer but how they function *in vivo* remains incompletely understood. Here, we combined intravital real-time imaging with single-cell RNA sequencing analysis and mouse models to uncover anti-PD-1 pharmacodynamics directly within tumors. We showed that effective antitumor responses required a subset of tumor-infiltrating dendritic cells (DCs), which produced interleukin 12 (IL-12). These DCs did not bind anti-PD-1 but produced IL-12 upon sensing interferon γ (IFN-γ) that was released from neighboring T cells. In turn, DC-derived IL-12 stimulated antitumor T cell immunity. These findings suggest that full-fledged activation of antitumor T cells by anti-PD-1 is not direct, but rather involves T cell:DC crosstalk and is licensed by IFN-γ and IL-12. Furthermore, we found that activating the non-canonical NF-κB transcription factor pathway amplified IL-12-producing DCs and sensitized tumors to anti-PD-1 treatment, suggesting a therapeutic strategy to improve responses to checkpoint blockade.

INTRODUCTION

Immune checkpoint blockade has emerged as a critical treatment against various cancer types (Topalian et al., 2012). Currently approved immune checkpoint blockers are monoclonal antibodies that target the cytotoxic T lymphocyte-associated protein 4 (CTLA-4) or programmed cell death protein 1 (PD-1) pathways. These inhibitory pathways are important because they protect the host from uncontrolled immune activation (Keir et al., 2008) but they can also be co-opted by tumors, which make them resist immune attack (Wherry, 2011). For instance, tumor-infiltrating cytotoxic $CD8^+$ T cells often express PD-1 that renders them ineffective against tumors. Consequently, anti-PD-1 (aPD-1) mAbs, or anti-PDL1 mAbs, are designed to antagonize the PD-1 inhibitory pathway in T cells and potentiate $CD8^+$ T cell-mediated tumor destruction.

To date, FDA-approved therapeutics targeting the PD-1-PDL1 signaling axis, in particular aPD-1 mAbs, have proved efficacious in the clinic among immune checkpoint blockade therapies. The ability of these drugs to drive sustained tumor control depends on several variables, including tumor infiltration by $CD8^+$ T cells (Galon et al., 2013; Huang et al., 2017), interferon-γ (IFN-γ) production (Schreiber et al., 2011; Ayers et al., 2017), neoantigen abundance (Rizvi et al., 2015), MHC class I expression (Marty et al., 2017; McGranahan et al., 2017), CD28 co-stimulatory signals (Hui et al., 2017; Kamphorst et al., 2017), patient microbiota (Matson et al., 2018; Routy et al., 2018), and antibody composition (Arlauckas et al., 2017; Dahan et al., 2015). However, we still have a limited understanding of how immune checkpoint blockers engage complex tumor microenvironments and which mechanisms define treatment success during the time when tumor rejection occurs.

To address these knowledge gaps, we sought to track key readouts of immunotherapy function *in vivo* at single-cell resolution (Pittet et al., 2018) and during tumor rejection, and we decipher how immune-mediated tumor control is achieved.

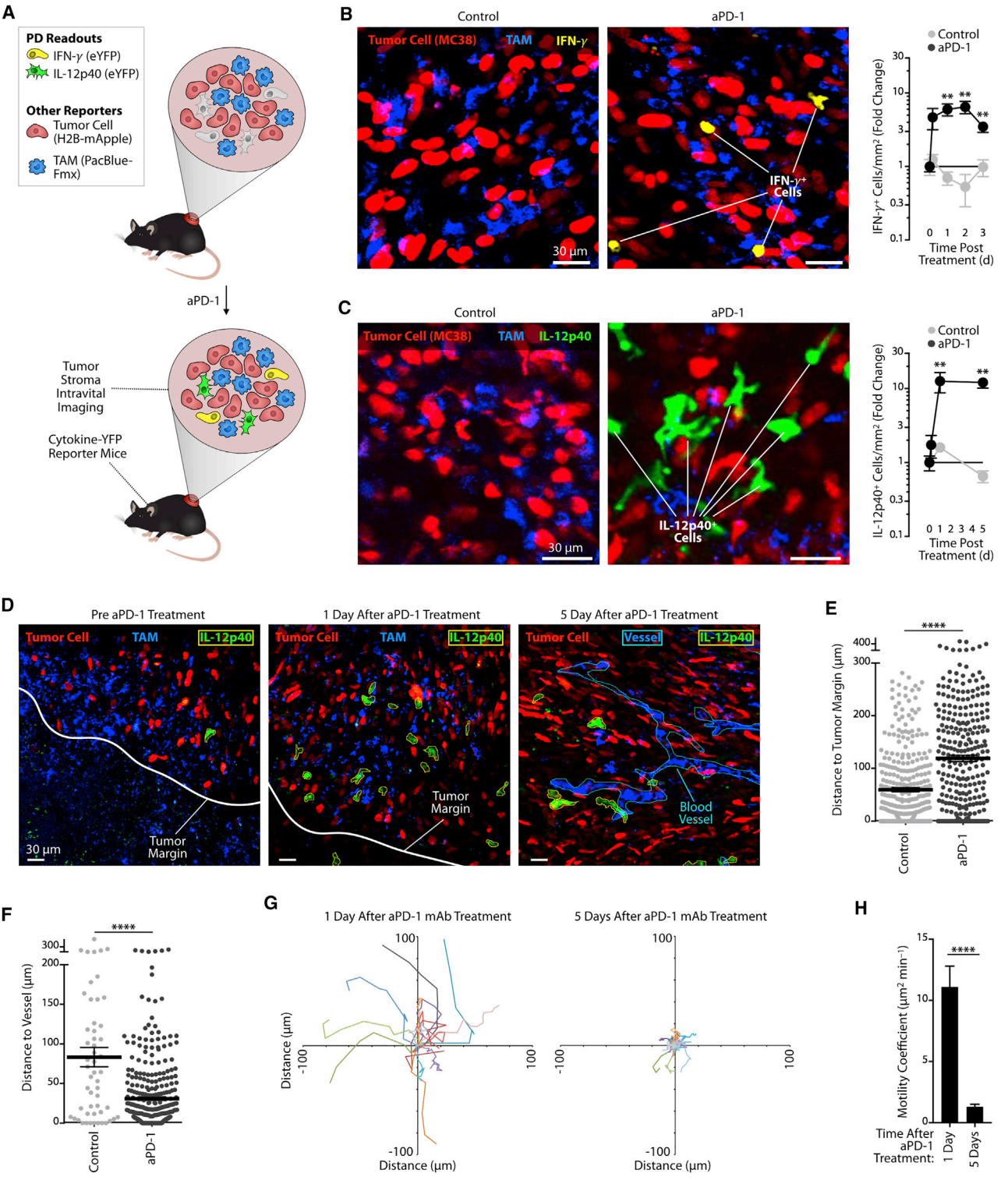

Figure 1. Successful aPD-1 Treatment Triggers Endogenous IFN-γ and IL-12 Responses within Tumors

(A) Diagram describing intravital imaging of MC38-H2B-mApple tumors implanted in cytokine-reporter mice for tracking lymphoid and myeloid cell pharmacodynamics (PD) after aPD-1 treatment.

(B) Left: Intravital micrographs of MC38 tumors in IFN-γ-eYFP reporter mice treated or not with aPD-1 mAb (n = 3 mice/group). Yellow, IFN-γ-eYFP-expressing cells; red, tumor cells; blue, PacificBlueFMX-labeled tumor-associated macrophages (TAM). Right: Fold change of IFN-γ$^+$ cells in both groups at different times after treatment and compared to baseline.

(C) Same as in (B) but in IL-12p40-eYFP reporter mice (n = 5 mice/group). Green, IL-12p40-eYFP-expressing cells; red, tumor cells; blue, TAM.

(legend continued on next page)

Considering that IFN-γ and interleukin 12 (IL-12) are key immune players in tissue-specific destruction (Galon et al., 2013; Nastala et al., 1994), we used intravital imaging to track these factors within tumors after aPD-1 treatment. Complementing single-cell imaging, we also used single-cell RNA sequencing (scRNAseq) to provide an unbiased view of immunotherapeutic responses across the tumor immune microenvironment.

These approaches, further combined with manipulations of the IFN-γ and IL-12 pathways *in vivo*, indicated that aPD-1 drove IL-12 production by a subset of tumor-infiltrating dendritic cells (DCs). Our imaging platform identified that DC activation was indirect (the drug did not detectably bind these cells *in vivo*) but required DC sensing of IFN-γ, which was produced by aPD-1-activated T cells. In turn, IL-12 produced by DCs licensed effector T cell responses. We further report that the non-canonical nuclear factor kappa-light-chain-enhancer of activated B cells (NF-κB) pathway was enriched within IL-12-producing DCs. This pathway was required for response to aPD-1, and agonizing it in a therapeutic setting enhanced IL-12 production by tumor-infiltrating DCs.

RESULTS

Successful aPD-1 Treatment Triggers Endogenous IFN-γ and IL-12 Responses within Tumors

To image key readouts of immunotherapy function, we assessed IFN-γ and IL-12p40, a protein subunit of IL-12 and IL-23, production using IFN-γ-internal ribosome entry site-yellow fluorescent protein (IFN-γ-IRES-YFP) and IL-12p40-IRES-YFP reporter mice, hereafter referred to as IFN-γ-eYFP and IL-12p40-eYFP, respectively (Figure 1A). Intravital imaging detects YFP, which is expressed by cells that have turned on IFN-γ or IL-12p40 production (Reinhardt et al., 2006, 2015). YFP remains detectable even after cytokine production is turned off, which makes intravital imaging a particularly useful tool to detect the activation of molecules with rapid on/off cycling, such as IFN-γ (Slifka et al., 1999). We tracked IFN-γ and IL-12p40 *in vivo* during rejection of aPD-1 treatment-sensitive MC38 tumor cells, which were labeled with H2B-mApple. We also tracked macrophages, which were tagged with Pacific-blue-dextran nanoparticles (Weissleder et al., 2014), as these cells are often abundant in tumors (Engblom et al., 2016).

Intravital imaging of the tumor microenvironment revealed a 6.0 ± 1.1 (mean ± SEM) fold expansion of IFN-γ-eYFP$^+$ cells 1 day after a single aPD-1 injection; this increase was sustained for up to 3 days after treatment (Figures 1B and S1A). IFN-γ-eYFP$^+$ cells accumulated within the tumor stroma and were mostly CD8$^+$ T cells (Figure S1B). Intravital imaging further revealed a 12.1- ± 3.7-fold increase of IL-12p40-eYFP$^+$ cells on day 1 after treatment, which persisted for at least 5 days (Figures 1C and S1C). IL-12p40-eYFP$^+$ cells displayed a branched morphology (mean circularity index: 0.54 ± 0.4), suggesting that they were DCs. In comparison to the few IL-12$^+$ cells detected before aPD-1 treatment, those present after treatment accumulated in deeper regions of the tumor (Figures 1D and 1E) and closer to vessels (Figure 1F). The ability for IL-12$^+$ cells to accumulate within tumors was supported by the real-time imaging observation that these cells were motile 1 day after aPD-1 treatment (motility coefficient: ~10 μm^2/min; Figures 1G and 1H and Video S1) and much less so on day 5 (<1 μm^2/min; Figures 1G and 1H and Video S2). These findings indicate that aPD-1 delivery to tumors functionally impacts at least two non-overlapping cell populations, which respond differently to treatment: CD8$^+$ T cells that activate the IFN-γ signaling pathway and DC-like cells that turn on IL-12 production.

scRNAseq Shows DC-Restricted IL-12 Production

We next sought to further characterize the aPD-1-induced IL-12$^+$ DC-like cells. Flow cytometry analysis confirmed these cells to be MHC class II$^+$ F4/80$^-$ (Figure S1D), and parabiosis of tumor-bearing mice indicated that these cells could derive from a blood-circulating precursor (Figure S1E). To provide a more comprehensive and unbiased view of immunotherapeutic responses across the tumor immune microenvironment, including all myeloid cell types, we performed scRNAseq analysis on CD45$^+$ cells isolated from untreated (n = 1,154 cells sequenced) or aPD-1-treated (n = 2,941 cells sequenced) tumors. All cells (n = 4,095) were clustered into unbiased cell type classifications using the Seurat single-cell analysis R package (Macosko et al., 2015). The cell clusters, visualized with t-stochastic neighbor embedding (t-SNE; Figures 2A and S2A) or force-directed graph layouts (SPRING) (Figure S2B; Weinreb et al., 2018), identified the following populations: conventional T (Tconv) cells expressing *Cd3e*, regulatory T (Treg) cells expressing the transcription factor forkhead box P3 (*Foxp3*), natural killer (NK) cells expressing natural cytotoxicity triggering receptor 1(*Ncr1*) and killer cell lectin-like receptor subfamily B member 1c (*Klrb1c*), neutrophils (Neu) expressing C-X-C motif chemokine receptor 2 (*Cxcr2*) and G0/G1 switch 2 (*G0s2*), monocytes (Mo) and macrophages (Macs) expressing colony stimulating factor 1 receptor (*Csf1r*), and two DC subsets, referred to as DC1 and DC2.

Both DC1s and DC2s expressed the DC markers *Batf3*, *Flt3*, *H2-Dmb2*, and *Zbtb46* (Meredith et al., 2012; Hildner et al., 2008); DC1s expressed *Fscn1* and *Ly75* (*DEC-205*); and DC2s expressed *CD209a* (*DC-SIGN*), *Mgl2* (*CD301b*), and *Cd24a* (Figures 2B and S2B). Both DC subsets were largely negative for the

(D) Representative intravital micrographs of H2B-mApple MC38 tumor edge or core obtained in IL-12p40 reporter mice before (left), 1 day after (middle), and 5 days after (right) aPD-1 treatment. PacBlue-labeled dextran was used to locate tumor vessels. Tumor cells, red; tumor-associated macrophages (TAM), blue; IL-12$^+$ cells, green with yellow contours; tumor margin, white; blood vessels, cyan. Scale bars represent 30 μm.

(E) Distance between IL-12p40$^+$ cells and the tumor margin measured by intravital imaging. Each point represents a single cell (n = 8 control and 5 aPD-1-treated mice).

(F) Distance between IL-12p40$^+$ cells and closest tumor vessel measured by intravital imaging. Each point represents a single cell (n = 5 mice/group).

(G) *In vivo* time-lapse microscopy of IL-12p40 reporter mice tracking IL-12$^+$ cell motility after aPD-1 treatment. Track plots represent displacement from origin of IL-12$^+$ cells in the tumor microenvironment.

(H) Motility coefficient was calculated for each IL-12$^+$ cell at both time points.

n.s., not significant; **p < 0.01, ****p < 0.0001. Error bar values represent SEM. Data are representative of at least two independent experiments. For comparisons between two groups, Student's two-tailed t test was used. See also Figure S1.

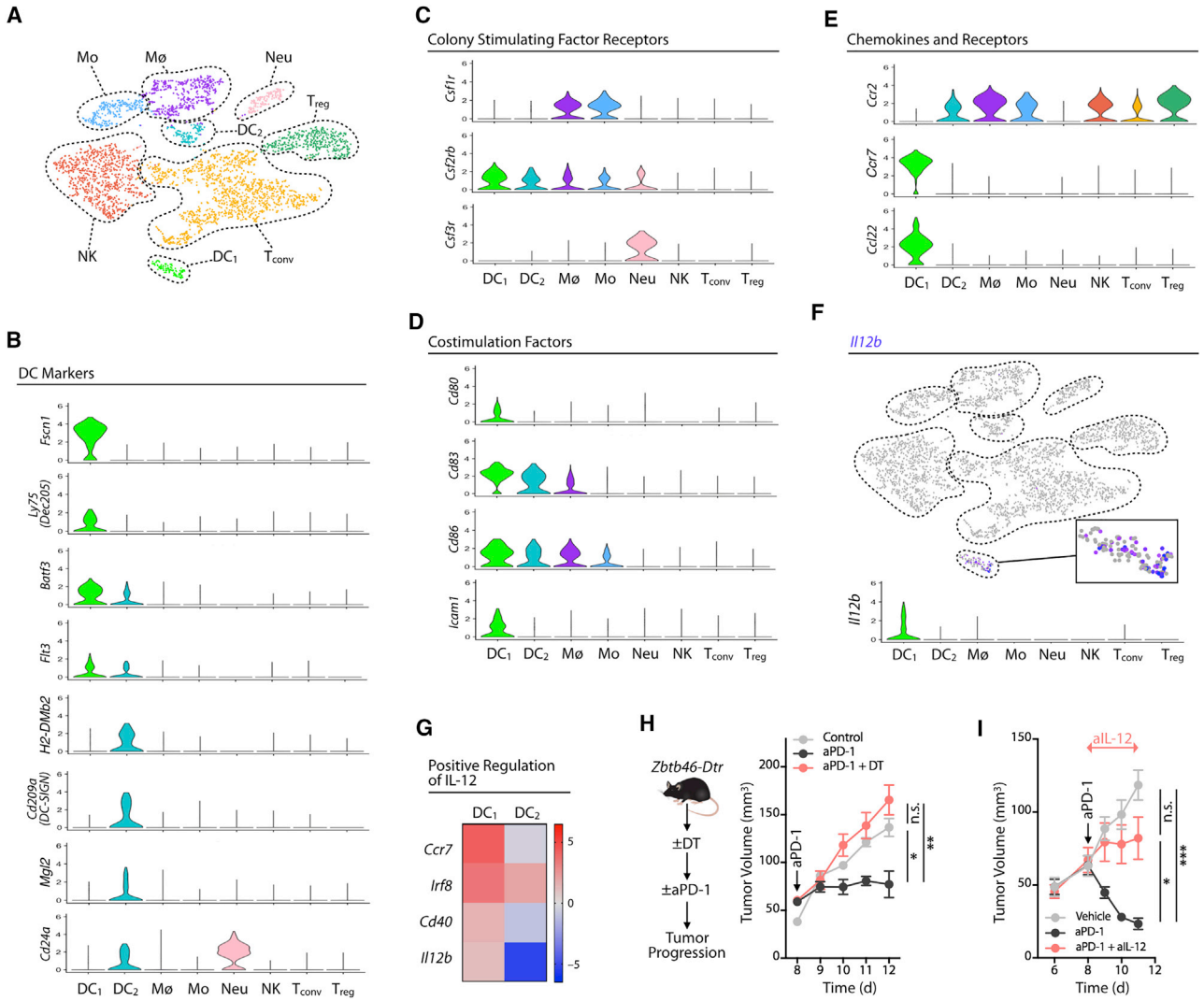

Figure 2. IL-12 Is Produced by DC1s and Is Necessary for Treatment Efficacy

(A) t-SNE plot using scRNAseq data from CD45$^+$ cells sorted from MC38 tumors 3 days after aPD-1 treatment. Untreated mice served as control. Control and aPD-1 samples are pooled.

(B–E) Violin plots showing the gene expression probability distribution of various dendritic cell markers (B), colony stimulating factor receptors (C), costimulation factors (D), and chemokine and chemokine receptors (E), in DC1, DC2, and other immune cell clusters (Macs, macrophages; Mo, monocytes; Neu, neutrophils; NK, natural killer cells; Tconv, conventional T cells; Treg, regulatory T cells).

(F) Feature plot of Il12b expression across cell clusters identified in (A).

(G) Expression in DC1 and DC2 of genes associated with IL-12 production.

(H) MC38 tumor volumes in Zbtb46-DTR bone marrow chimeras treated or not with diphtheria toxin (DT) to deplete DCs prior to aPD-1 or control treatment.

(I) MC38 tumor volume in mice treated with aPD-1 (black), aPD-1 and aIL-12 (red), or vehicle (gray); n = 15 mice/group.

Data are representative of at least two independent experiments. Arrows indicate duration of treatment. n.s., not significant; *p < 0.05, ***p < 0.001. Error bar values represent SEM. For comparisons between three or more groups, one-way ANOVA with multiple comparisons was used. See also Figure S2.

macrophage colony-stimulating factor receptor *Csf1r* (Figure 2C), although some DC2s expressed this receptor (Figure S2A), similarly to a subset of intratumoral DCs previously reported (Broz et al., 2014). DC1s had higher expression of the granulocyte/macrophage colony-stimulating factor receptor *Csf2rb* compared to DC2s, and neither DC1s nor DC2s expressed the granulocyte colony-stimulating factor receptor *Csf3r* (Figure 2C). Additionally, DC1s were enriched for the T cell co-stimulatory factors *Cd80*, *Cd83*, *Cd86*, and *Icam1* (Figure 2D), and DC1s and DC2s expressed distinct chemokines and chemokine receptors (Figure 2E).

IL-12p40 (also known as IL12b) expression was contained exclusively within the DC1 population (Figure 2F). Curating genes defined from gene ontology for positive regulation of IL-12 signaling and synthesis (GO:0045084, 0032735), we found that DC1s were enriched in IL-12-related production factors such as *Cd40* and *Irf8* (Figure 2G). IL-12$^+$ DCs in MC38 tumors did not express *Itgae* (the gene encoding the integrin CD103)

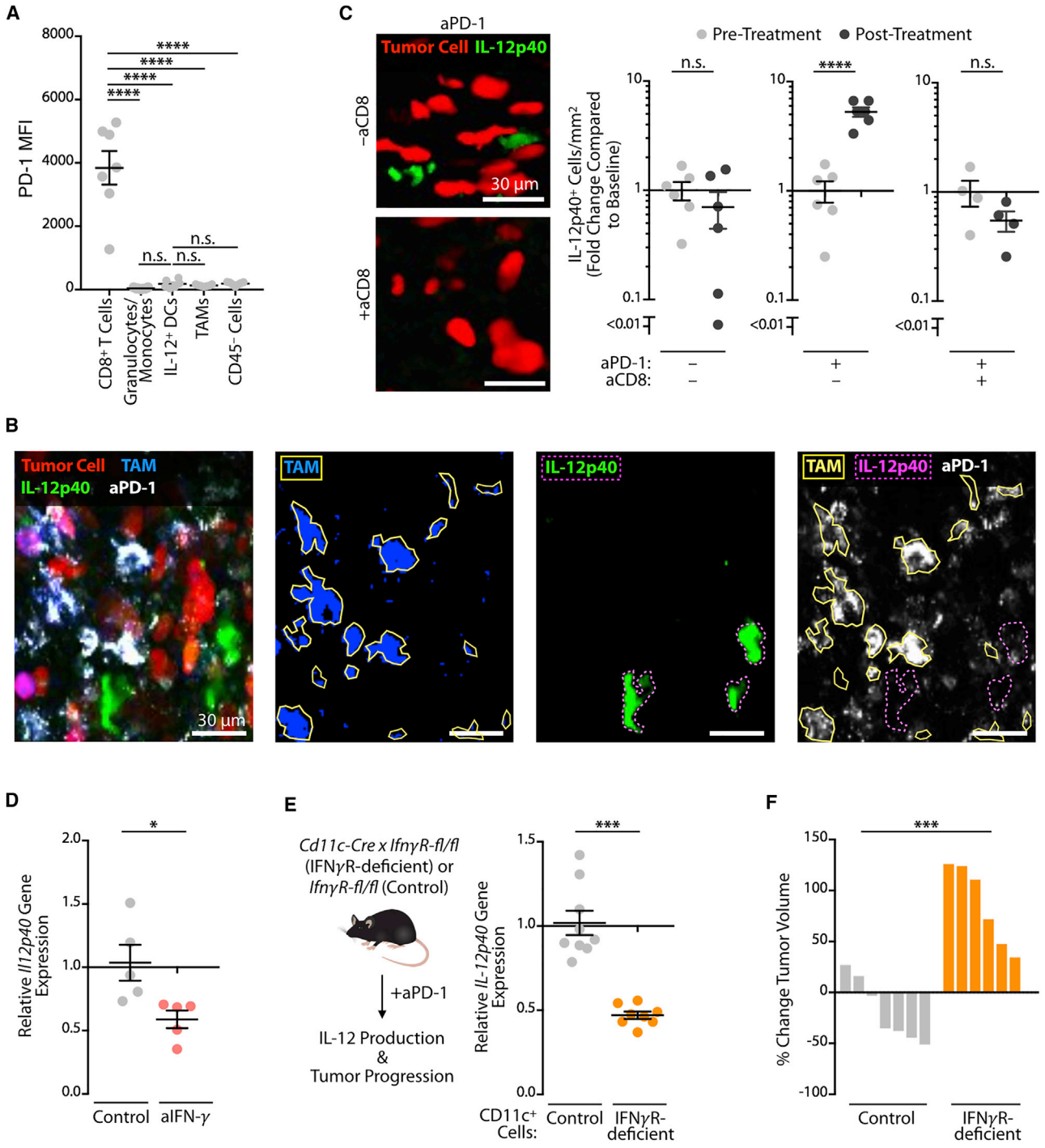

Figure 3. DC-Mediated IL-12 Production Requires IFN-γ Sensing

(A) Flow cytometry measurement of PD-1 expression across cell types in the MC38 tumor microenvironment.

(B) Intravital micrographs of the MC38 tumor microenvironment in an IL12 reporter mouse 5 days after AF647-aPD-1 treatment. Tumor cells (red), TAM (blue), IL-12p40 (green), aPD-1 (white).

(C) Intravital micrographs and quantification of IL-12p40 signal 2 days after aPD-1 treatment in the tumor microenvironment after CD8 depletion. Tumor cells (red), IL-12p40 (green). Data plotted as fold change in IL-12p40 from baseline levels.

(D) MC38 tumors were harvested at 3 days post-treatment with aPD-1 in combination with aIFN-γ or control, and processed for RNA isolation. Quantitative PCR for IL12p40 gene expression data are normalized with control sample values set to 1.

(E) Relative IL-12p40 gene expression in MC38 tumors from CD11c-cre (Itgax-cre) × IFN-γR1$^{fl/fl}$ (IFN-γR-deficient) or control (IFN-γR1$^{fl/fl}$) mice 3 days after aPD-1 treatment.

(legend continued on next page)

(Figure S2C), although previous studies identified CD103$^+$ DCs as important cells for immune responses to tumors (Salmon et al., 2016; Spranger et al., 2015; Ruffell et al., 2014; Broz et al., 2014). This discrepancy may be due to tissue location, as we found that IL-12$^+$ DCs expressed CD103 in lung tumor models (Figure S2D). scRNaseq analysis confirmed the expansion of IL-12$^+$ DCs after aPD-1 treatment (Figure S2E). Collectively, these data demonstrate a distinct population of IL-12-producing DCs in the tumor microenvironment.

DCs and IL-12 Are Relevant to aPD-1 Therapy

To assess whether DCs are relevant to aPD-1 treatment, we generated *Zbtb46-DTR* bone marrow chimeras (Meredith et al., 2012), which allowed us to deplete DCs selectively and do so after tumors were established but before aPD-1 treatment was initiated. Mice lacking DCs failed to reject tumors in response to aPD-1 (Figure 2H), indicating that these cells were required at the time when aPD-1-mediated tumor rejection occurs. To define whether IL-12 contributes to aPD-1 therapeutic efficacy, we studied DC-sufficient MC38 tumor-bearing mice that received aPD-1 in the presence or absence of neutralizing IL-12 mAbs. Mice in which IL-12 was neutralized failed to reject tumors, indicating that IL-12 production after aPD-1 treatment was necessary for achieving tumor control (Figure 2I). Collectively, these data indicate that aPD-1 treatment induces IL-12 production by DCs and that both DCs and IL-12 critically regulate aPD-1 treatment potency. The results accord with previous findings that tumor-infiltrating DCs can foster T cell immunity (Broz et al., 2014; Salmon et al., 2016) and immunotherapeutic responses (Alloatti et al., 2017), and here we show that DCs assist antitumor responses by providing cytokine support to the tumor immune microenvironment.

IFN-γ Sensing by DCs Controls IL-12 Production

To define how aPD-1 treatment activates DCs, we asked initially whether the antibody binds to these cells directly. Some myeloid cells have been proposed to express PD-1 (Gordon et al., 2017); however, both flow cytometry and scRNAseq analyses indicated that IL-12$^+$ DCs did not express the PD-1 receptor at both transcript (Figure S2A) and protein (Figure 3A) levels. We further tested whether aPD-1 antibodies bind IL-12$^+$ DCs independently of PD-1. Indeed, aPD-1 mAbs initially accumulate on PD-1$^+$ T cells but can then be gradually taken up by tumor-associated macrophages (TAMs) in a FcγR-dependent manner (Arlauckas et al., 2017). However, IL-12$^+$ DCs did not express detectable levels of FcγR transcripts, in contrast to TAMs (Figure S3A). Also, when tracking the drug's pharmacokinetics by intravital imaging in MC38 tumor-bearing IL-12-reporter mice, we confirmed aPD-1 accumulation in TAMs but not in IL-12$^+$ DCs 24 hr after aPD-1 administration (Figures 3B and S3B). The DCs also failed to bind aPD-1 early after drug administration, i.e., before uptake by TAMs (Figure S3C). Based on these data, we concluded that it was unlikely for aPD-1 to bind and activate IL-12$^+$ DCs directly.

As aPD-1 mAbs physically bind to tumor-infiltrating CD8$^+$ T cells (Arlauckas et al., 2017), we hypothesized that these cells, once activated by aPD-1, could promote IL-12 production by DCs. To address this possibility, we used intravital imaging to track IL-12 expression in mice depleted of CD8$^+$ T cells prior to administration of aPD-1. Absence of CD8$^+$ T cells abrogated IL-12 production (Figure 3C). We further reasoned that IFN-γ could mediate IL-12 production by DCs, since this cytokine was produced by aPD-1-activated CD8$^+$ T cells (Figure 1B) and can enhance IL-12 responses (Ma et al., 1996). To test this hypothesis, we assessed mice in which IFN-γ was neutralized during aPD-1 treatment. We found that IFN-γ blockade reduced IL-12 production within the tumor microenvironment (Figure 3D). Decreased IL-12 production by DCs (Figure S3D) and decreased numbers of IL-12$^+$ DCs (Figures S3E and S3F) both contributed to this reduction. Consequently, IFN-γ blockade prevented aPD-1-mediated MC38 tumor control (Figure S3G).

The above results suggest that IFN-γ sensing by DCs fosters IL-12 production and results in tumor control. To test this hypothesis directly, we eliminated DC sensing of IFN-γ by crossing *Itgax*-cre with *Ifngr1*$^{fl/fl}$ mice (Lee et al., 2013). Tumors from these mice showed impaired IL-12p40 production (Figure 3E) and were unresponsive to aPD-1 treatment (Figure 3F), underscoring the importance of IFN-γ sensing by DCs, and potentially other CD11c-expressing cells, during aPD-1 therapy. Prior studies of *Ifngr1*-deficient DCs (Nirschl et al., 2017) described downregulation of genes such as *Fscn1*, *Ccr7*, and *Icam1*, which we identified as IL-12$^+$ DCs distinguishers by scRNAseq analysis (Figures 2B, 2D, and 2E). Together, we find an indirect aPD-1 effect on DCs; this effect was mediated through IFN-γ and is critical for IL-12 induction and, consequently, treatment response.

IL-12 Activates Tumor-Infiltrating Lymphocyte Effector Functions in Mice

Our investigations indicated that aPD-1 treatment elicits both IFN-γ and IL-12 responses at the tumor site. By contrast, we did not find evidence of IFN-γ or IL-12 induction by aPD-1 in the local draining lymph node (Figures S4A and S4B), suggesting that the checkpoint blockade response occurs within tumors. Consistent with this notion, scRNAseq data indicated that aPD-1 treatment triggered the proliferation of tumor-infiltrating CD8$^+$ T cells (Figure S4C). Furthermore, blocking lymphocyte recirculation through treatment with the trafficking inhibitor FTY720 did not affect the antitumor response to aPD-1 treatment (Figures S4D and S4E). These data suggest that pre-existing tumor-infiltrating T cells are sufficient for driving the response to aPD-1 at least in this model.

We next examined the downstream effects of IL-12 production within the tumor microenvironment. Initially we used intravital microscopy to assess the effects of recombinant IL-12 administered to tumors in IFN-γ reporter mice (in the absence of aPD-1). We found that intratumoral IL-12 substantially expanded IFN-γ-eYFP$^+$ cells (5.9- ± 0.7-fold increase by day 4; Figure 4A). Consistent with previous reports (Nastala et al., 1994), IL-12 administration to MC38 tumors produced robust antitumor

(F) Change in MC38 tumor volume on day six after aPD-1 treatment in IFN-γR-deficient or control mice.

Data are relative to pre-treatment tumor volumes. Data are representative of at least two independent experiments. n.s., not significant; *p < 0.05, **p < 0.01, ***p < 0.001, ****p < 0.0001. Error bar values represent SEM. For comparisons between two groups, Student's two-tailed t test was used. For comparisons between three or more groups, one-way ANOVA with multiple comparisons was used. See also Figure S3.

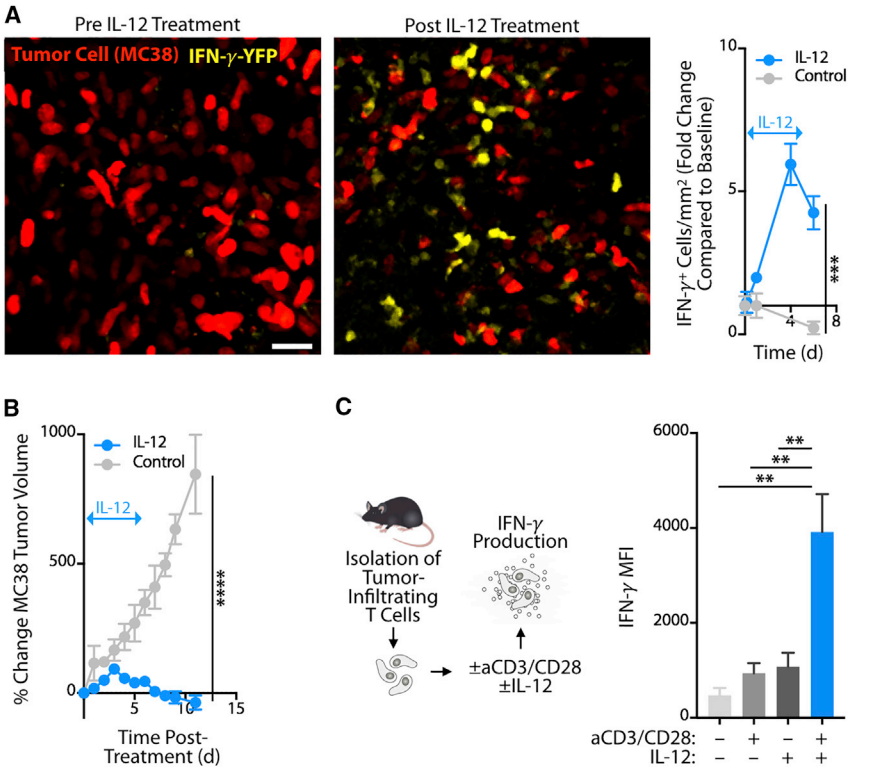

Figure 4. IL-12 Activates TILs Directly in Mice

(A) Left: Intravital micrographs of MC38 tumors in IFN-γ-eYFP reporter mice before or 4 days after treatment with recombinant IL-12. Yellow, IFN-γ-eYFP-expressing cells; red, MC38 tumor cells. Right: Fold change of IFN-γ$^+$ cells in treated and untreated groups compared to baseline. Arrow indicates duration of IL-12 treatment.

(B) MC38 tumor growth monitored after mice bearing established tumors were treated with recombinant IL-12 (blue line) or control (gray line) for 5 days; n ≥ 3 per group.

(C) Tumor-infiltrating CD8$^+$ T cells isolated from MC38 tumors, stimulated *in vitro* with anti-CD3/CD28 and/or IL-12, and assessed by flow cytometry for intracellular IFN-γ production.

Data show IFN-γ mean fluorescent intensity (MFI; n = 3 per group). Data are representative of at least two independent experiments. **p < 0.01, ***p < 0.001, ****p < 0.0001. Error bar values represent SEM. For comparisons between two groups, Student's two-tailed t test was used. For comparisons between three or more groups, one-way ANOVA with multiple comparisons was used. See also Figure S4.

responses (Figure 4B). To test further whether IL-12 can activate tumor-infiltrated CD8$^+$ T cells directly, we isolated these cells from MC38 tumors and subjected them to aCD3/CD28 stimulation with or without IL-12. Stimulated CD8$^+$ T cells substantially increased IFN-γ production in the presence of IL-12 (Figure 4C), indicating that tumor-infiltrating T cells can respond to IL-12 directly. The requirement for both T cell co-stimulation and IL-12 to achieve maximal IFN-γ response likely reflected the need of CD28 to rescue exhausted CD8$^+$ T cells and possibly also the role of PD-1 in limiting CD28-mediated co-stimulation (Kamphorst et al., 2017; Hui et al., 2017).

IL-12 Activates Tumor-Infiltrating Lymphocyte Effector Functions in Cancer Patients

We next addressed the downstream effects of IL-12 in cancer patients using two clinical cohorts. First, to assess IL-12's effects within tumors, we collected skin tumor biopsies from 19 melanoma patients both before and after intratumoral treatment with ImmunoPulse tavokinogene telseplasmid, an electroporation method that delivers plasmid IL-12 directly to tumors (Daud et al., 2008). Comparison of pre- and post-treatment samples revealed that IL-12 delivery enhanced expression of core cytolytic genes (Rooney et al., 2015) within tumors (Figures 5A and 5B). These genes, namely *CD2*, *CD3E*, *CD247*, *GZMA*, *GZMH*, *GZMK*, *NKG7*, and *PRF1*, are associated with immunoediting and antitumor immune responses (Rooney et al., 2015) and tumors enriched with these genes are more likely to respond to aPD-1 immunotherapy (Riaz et al., 2017). Accordingly, we observed a positive association between enhanced cytolytic gene signature and therapeutic response in these patients (Figure 5C). *IFNG* was not detectably increased in the post-treatment samples, which is expected from the timing of tissue collection and rapid on/off cycling of IFN-γ production by T cells (Slifka et al., 1999). These observations indicated that IL-12 can induce cytolytic activity in human tumors.

To define whether IL-12 can directly activate human tumor-infiltrating CD8$^+$ T cells upon isolation of these cells, we collected fresh tumor tissue from six cancer patients, which included two lung adenocarcinomas (patients BS728 and LA061), three lung squamous cell carcinomas (patients BS469, BS698, and BS705), and one synovial sarcoma (patient BS661). CD8$^+$ T cells were purified from all tumors *ex vivo* (Figure S5) and subjected to aCD3 stimulation with or without IL-12. The presence of IL-12 increased IFN-γ production by CD8$^+$ T cells in five out of six patients (Figure 5D). Collectively, these patient data recapitulate our observations in mice that IL-12 can directly stimulate tumor-infiltrating T cell antitumor activity. They also support previous evidence that CD8$^+$ T cell activation within tumors is critical to antitumor activity (Broz et al., 2014; Spranger et al., 2014).

Activation of the Non-canonical NF-κB Pathway Amplifies IL-12-Producing DCs

On account of IL-12's ability to license antitumor T cell immunity, we further asked whether agonizing IL-12-producing cells could augment response to aPD-1 therapy. We examined the non-canonical NF-κB pathway as a therapeutic target, considering its relevance for priming cytotoxic T cells (Katakam et al., 2015; Lind et al., 2008) and because key non-canonical NF-κB pathway genes, namely *Cd40*, *Birc2* (*Ciap1*), *Map3k14* (*Nik*), *Nfkb2* (*p100*), and *Relb*, were all selectively upregulated in the IL-12$^+$ tumor-infiltrating DC subset (Figure 6A). We confirmed that IL-12$^+$ cells had more cell surface CD40 than their IL-12$^-$ counterparts (Figure S6A) and that IL-12$^+$ DCs expressed more CD40 than tumor-associated macrophages (Figure S6B).

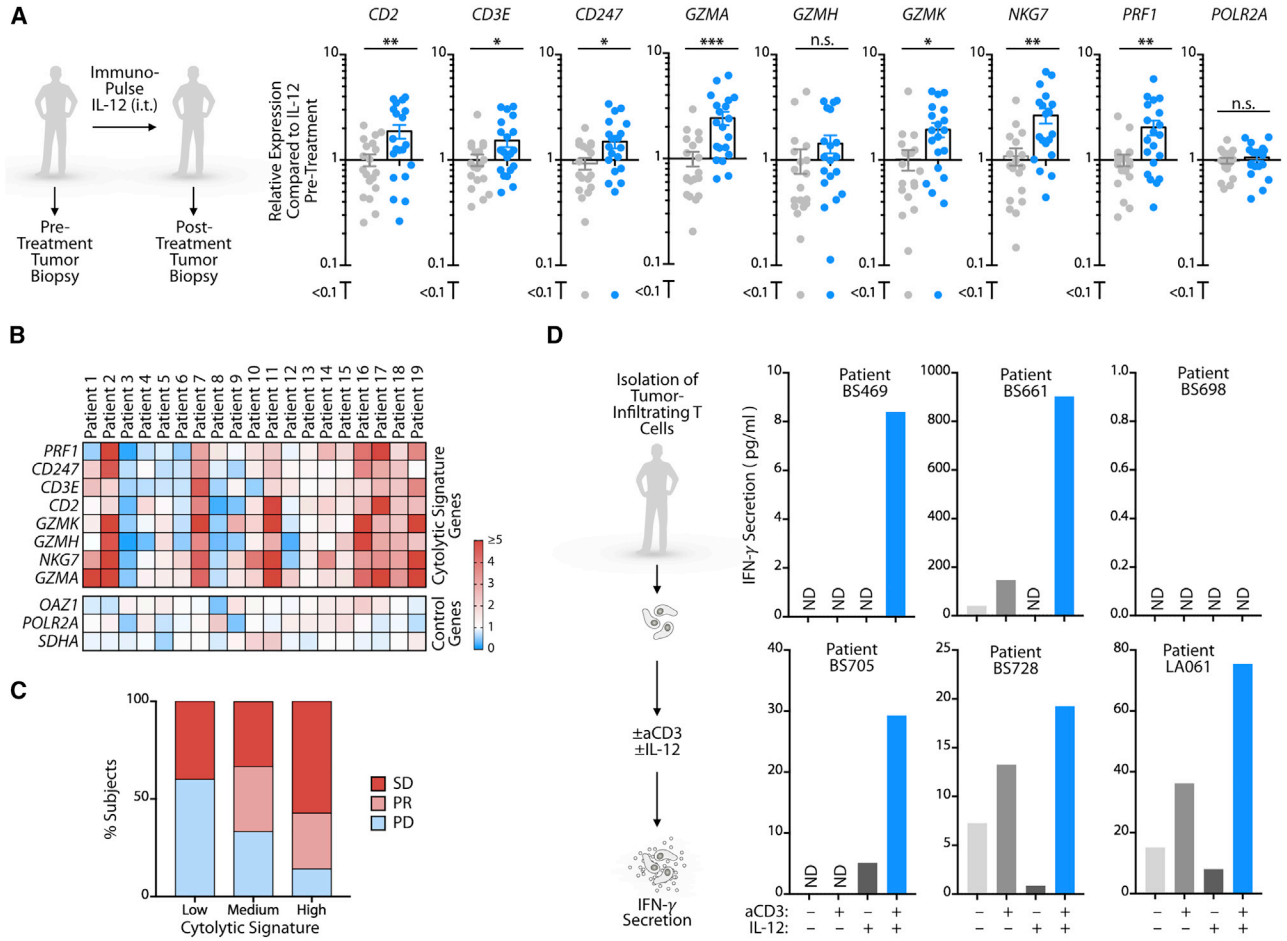

Figure 5. IL-12 Activates TILs Directly in Cancer Patients

(A) Relative expression levels of cytolytic signature genes measured by Nanostring in skin tumor biopsies from 19 melanoma patients both before (gray dots) and after (blue dots) intratumoral treatment with ImmunoPulse IL-12. Data are normalized to pre-treatment biopsy expression levels; POL2RA is a control gene.

(B) Heatmap of individual patient gene expression from melanoma biopsies from (A). Cytolytic signature genes are displayed as fold change over pre-treatment levels for each individual patient. OAZ1, POLR2A, and SDHA are control genes.

(C) Clinical outcomes data from patients receiving ImmunoPulse treatment. SD, stable disease; PR, partial response; PD, progressive disease. Cytolytic signature was calculated as the sum of total cytolytic gene signature expression from (B). Values were stratified by the top, middle, and bottom third, and then associated to patient response status.

(D) IFN-γ production by tumor-infiltrating $CD8^+$ T cells isolated from six cancer patients, stimulated *ex vivo* with aCD3 and/or IL-12, and measured by ELISA.

n.s., not significant; ND, not detected; $^*p < 0.05$, $^{**}p < 0.01$, $^{***}p < 0.001$. Error bar values represent SEM. For comparisons between two groups, Student's two-tailed t test was used. See also Figure S5.

We sought to activate the non-canonical NF-κB pathway in two different ways: with agonistic CD40 mAbs that have previously shown antitumor activity (Beatty et al., 2011; Byrne and Vonderheide, 2016) or with the small molecule inhibitor AZD5582 that targets cellular inhibitor of apoptosis protein (cIAP) 1 and 2 (Hennessy et al., 2013). Agonistic aCD40 mAbs were labeled with a fluorescent dye and tracked by intravital microscopy within tumors of IL-12 reporter mice. This imaging approach not only showed the drug's ability to interact directly with $IL\text{-}12^+$ tumor-infiltrating cells, and some macrophages, *in vivo* (Figure 6B) but further identified that the treatment induced a 6.6- ± 1.2-fold increase of tumor-infiltrating $IL\text{-}12^+$ cells (Figure 6C). Flow cytometry measurements indicated that IL-12 was produced by DCs but not TAMs (Figures 6D and 6E). These findings align with previous evidence that aCD40 therapy relies upon Batf3-dependent DCs (Byrne and Vonderheide, 2016), although macrophages can also contribute to aCD40 therapy in some settings, which may be independent of IL-12 (Hoves et al., 2018; Beatty et al., 2011).

CD40, in addition to activating myeloid cells, is also a well-known activator of B cells. Therefore, we tested whether B cells were important for aCD40 therapy response. We found that B cell depletion had no effect on aCD40 therapy, suggesting that B cells are not necessary for aCD40 treatment in this experimental model (data not shown).

Treating tumors with the cIAP antagonist AZD5582 induced a 4.0- ± 1.3-fold increase of $IL\text{-}12^+$ tumor-infiltrating cells (Figure 6C), similar to the effects observed with agonistic CD40 mAbs. Furthermore, stimulation of Flt3L-derived bone marrow DCs with AZD5582 potently enhanced IL-12 production *in vitro*

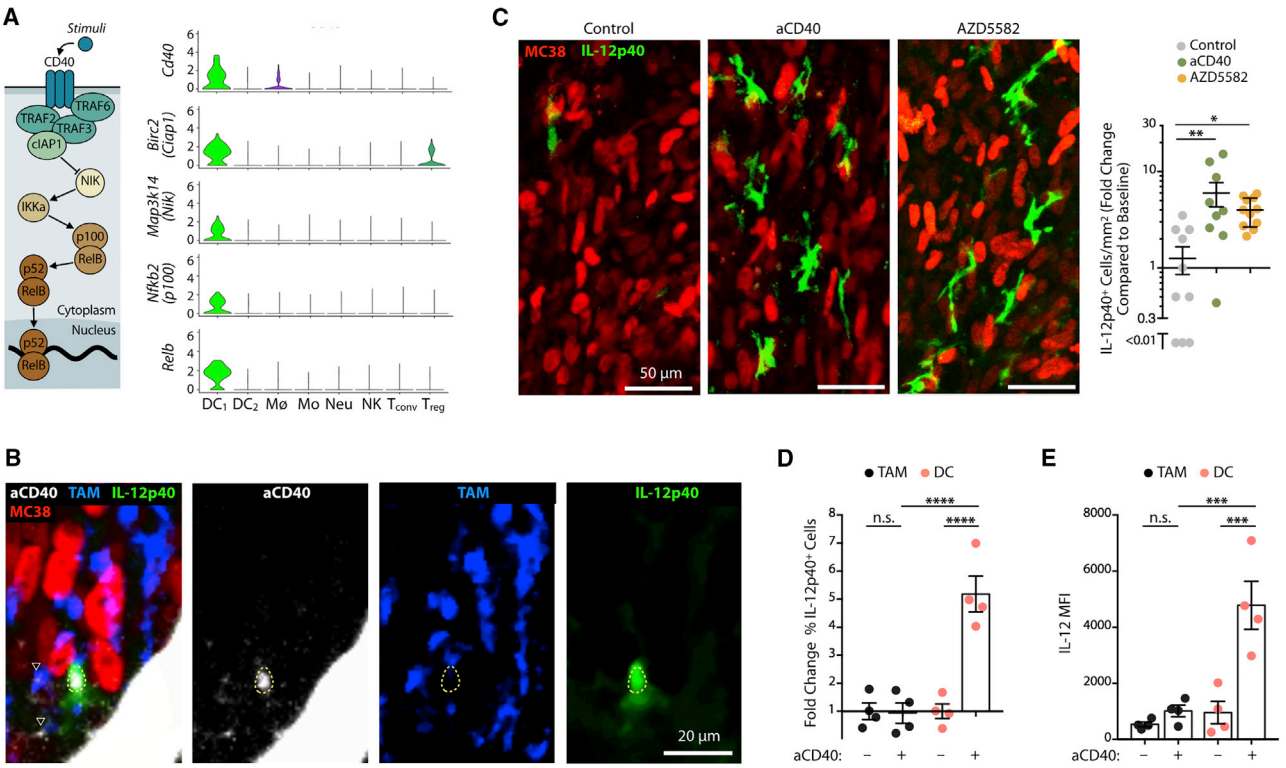

Figure 6. Molecular Targeting of the Non-canonical NF-κB Pathway Stimulates IL-12-Producing DCs

(A) Expression of non-canonical NF-κB pathway components (illustrated on the left) across immune populations.

(B) Intravital micrographs of a MC38 tumor in an IL-12p40 reporter mouse treated with AF647-aCD40 mAbs. Tumor cells (red), AF647-aCD40 (white), IL-12p40 (green), TAM (blue). Dashed yellow line highlights the location of an IL-12p40$^+$ cell; open arrowheads show TAM overlaying with aCD40 mAbs.

(C) Left: Intravital micrographs of MC38 tumors in IL-12p40-eYFP reporter mice treated with aCD40 or AZD5582. Untreated mice were used as controls. Green, IFN-γ-eYFP-expressing cells; red, tumor cells. Right: Fold change of IL-12p40$^+$ cells in each group after 48 hr and compared to baseline.

(D and E) *Ex vivo* flow cytometry analysis of MC38 tumors in IL-12p40 reporter mice treated or not 48 hr prior with agonistic aCD40 mAbs. CD45$^+$F4/80$^+$ TAMs (black) and CD45$^+$F4/80$^-$CD11c^{hi} MHCIIhi DCs (red).

(D) Fold change of IL-12p40$^+$ cells normalized to untreated mice.

(E) MFI of IL-12 reporter signal from TAM or DC.

Data are representative of at least two independent experiments. n.s., not significant; *p < 0.05, **p < 0.01, ***p < 0.001, ****p < 0.0001; one-way ANOVA with multiple comparisons. Error bar values represent SEM. See also Figure S6.

(Figure S6C). These results not only confirm previous evidence that CD40 agonism is a stimulatory signal for DCs (Cella et al., 1996; Ngiow et al., 2016) but also indicate that triggering the non-canonical NF-κB pathway, through CD40 agonism or cIAP inhibition, can amplify IL-12$^+$ tumor-infiltrating DCs.

Amplification of IL-12$^+$ DCs Improves Cancer Immunotherapy in an IL-12-Dependent Manner

The antitumor activity of agonistic CD40 mAbs (aCD40) has been shown to depend upon IFN-γ (Byrne and Vonderheide, 2016). We evaluated aCD40 in IFN-γ reporter animals and indeed found that aCD40 treatment potently enhanced intratumoral IFN-γ levels (Figure 7A). The IFN-γ induction by aCD40 likely occurred indirectly as T cells did not express CD40 (Figure 6A). Furthermore, treatment with either agonistic aCD40 mAbs or AZD5582 provided antitumor effects *in vivo* (Figure 7B). To test the relevance of IL-12 after treatments with aCD40 or AZD5582, we compared their effects in MC38 tumor-bearing mice that were administered or not with IL-12 neutralizing mAbs. These studies showed that IL-12 induction was a primary mechanism for these treatments because tumor control was lost in animals receiving IL-12 neutralizing mAbs (Figure 7B). To further assess the requirement of non-canonical NF-κB signaling to aPD-1 treatment efficacy, we compared aPD-1 responses in mice that were reconstituted with either *Map3k14* (NIK)-deficient or wild-type bone marrow. NIK chimeras failed to respond to aPD-1 (Figure S7A). Taken together, these data linked the non-canonical NF-κB pathway to antitumor intratumoral DCs and to aPD-1 treatment efficacy and indicated that targeting non-canonical NF-κB components can be therapeutic in cancer.

Next we defined whether agonizing IL-12$^+$ cells could augment response to aPD-1 therapy. To this end, we assessed MC38 tumor progression in mice treated with antagonist aPD-1, agonist aCD40, or both. We found that monotherapies incompletely controlled tumor growth, whereas the combination treatment produced a complete, durable response in most animals treated (Figures 7C, S7B, and S7C). Mice that received combination treatment further resisted tumor re-challenge 8 weeks after the primary tumor rejection (Figure S7D); this indicated that the treatment had triggered antitumor memory.

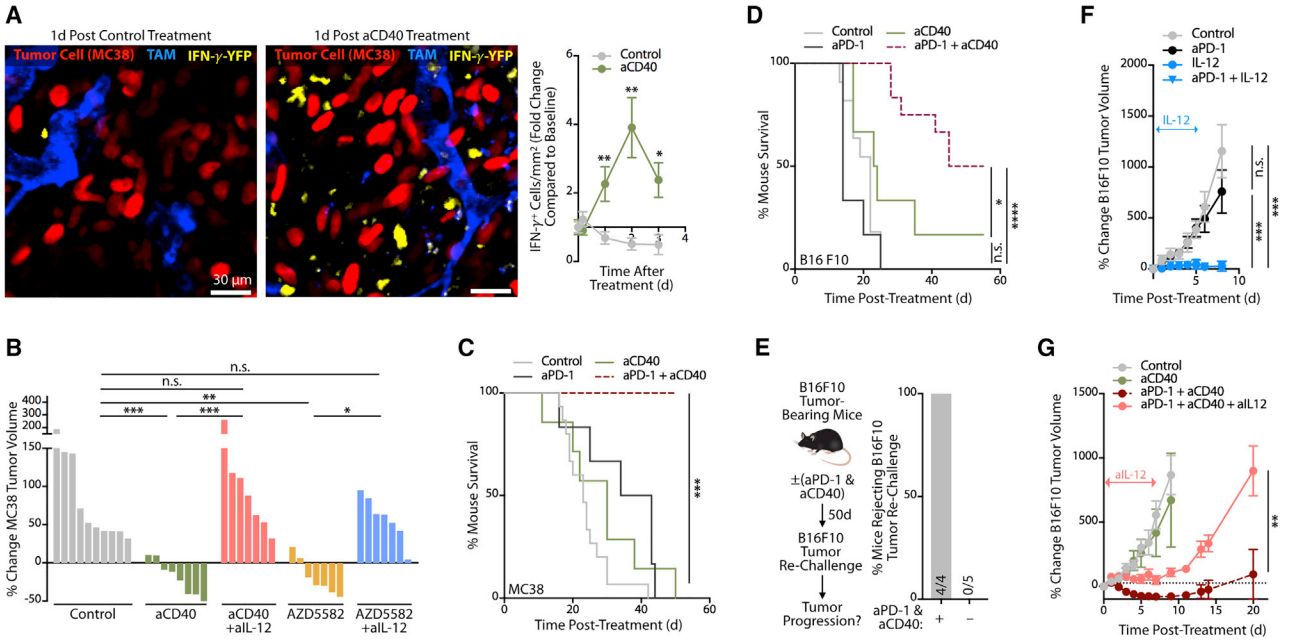

Figure 7. Amplification of IL-12-Producing DCs Improves Cancer Immunotherapy in an IL-12-Dependent Manner

(A) Intravital images of MC38 tumors in IFN-γ reporter mice treated with control mAb (left) or agonistic aCD40 mAb (middle). Images were recorded 1 day after treatment. Red, MC38 tumor cells; blue, tumor-associated macrophages (TAM); yellow, IFN-γ-producing cells. Scale bars represent 30 μm. Longitudinal imaging of control or aCD40-treated mice was used to quantitate the change in density of IFN-γ-expressing cells compared to pre-treatment (right). For both mouse cohorts, at least ten fields of view per time point were used.

(B) MC38 tumor volume change after aCD40 or AZD5582 treatment in MC38 tumor-bearing mice with or without neutralizing IL-12 mAbs (aIL-12). Data are normalized to pre-treatment tumor volumes for individual mice, n = 7–9 mice/group.

(C) Survival of MC38 tumor-bearing mice treated with aCD40 (green), aPD-1 (black), or aPD-1 + aCD40 (red). Untreated mice served as controls (gray), n ≥ 6 mice/group.

(D) Survival of B16F10 melanoma tumor-bearing mice treated with aCD40 (green), aPD-1 (black), or aPD-1 + aCD40 (red). Untreated mice served as controls (gray), n = 7–12 mice/group.

(E) Mice cured with aPD-1 + aCD40 (see F) were re-challenged ~50 days later with B16F10 melanoma cells. Naive mice challenged at the same time served as positive controls. Data show the percent of mice rejecting B16F10 tumor re-challenge in each group.

(F) Change in B16F10 tumor volume after treatment with aPD-1 (black circles), IL-12 (blue circles), or both (blue triangles). Untreated mice served as controls (gray circles), n ≥ 5 mice/group.

(G) Change in B16F10 tumor volume following treatment with aCD40 (green line), aPD-1 + aCD40 (red dashed line), or aPD-1 + aCD40 + aIL-12 (pink line). Untreated mice served as controls (gray circles), n ≥ 5 mice/group.

Data are representative of at least two independent experiments. n.s., not significant; *p < 0.05, **p < 0.01, ***p < 0.001, ****p < 0.0001. Error bar values represent SEM. For comparisons between two groups, Student's two-tailed t test was used. For comparisons between three or more groups, one-way ANOVA with multiple comparisons was used. See also Figure S7.

Because the MC38 tumor model responds—though not completely—to aPD-1 monotherapy, we also tested the B16F10 melanoma model, which resists aPD-1 treatment. We found that combining aPD-1 with aCD40 mAbs controlled B16F10 tumor growth (Figures S7E and S7F) and resulted in increased mouse survival (Figure 7D), when compared to aPD-1 or aCD40 monotherapies. The combination treatment rejected tumors in 50% (6 of 12) mice; these mice resisted secondary tumor challenge (Figure 7E), indicating that the treatment had also triggered antitumor memory in this model.

Considering that recombinant IL-12 administered to B16F10 melanoma-bearing mice also produced a substantial antitumor effect (Figure 7F), we tested whether the aPD-1+aCD40 therapeutic combination relied upon IL-12 for activity. We administered the combination immunotherapy to B16F10-bearing mice in the presence or absence of IL-12 neutralizing mAbs and found that blocking IL-12 signaling prevented the combination treatment's therapeutic activity (Figures 7G and S7G). These data indicate that DC targeting can augment immunotherapy efficacy and sensitize tumors to aPD-1 treatment in an IL-12-dependent manner.

DISCUSSION

We used single-cell resolution readouts, including intravital microscopy and scRNAseq, to discover cancer immunotherapy pharmacodynamics within tumors and better define *in vivo* mechanisms of tumor rejection. We found that the antitumor cytokines IFN-γ and IL-12 were mutually induced by immunotherapy and further distinguished direct and indirect mechanisms of activation for these respective cytokines. Principally, we identified that aPD-1 directly induced IFN-γ production by activated T cells, but indirectly induced IL-12 production by a subset of intratumoral DCs. IL-12 production required DC

sensing of IFN-γ, and, in turn, licensed effector T cell responses in both mice and cancer patients. We also showed that IL-12-producing DCs were enriched for non-canonical NF-κB signaling pathway components, that the critical non-canonical NF-κB kinase NIK was required for aPD-1 response, and that agonism of the non-canonical NF-κB pathway in a therapeutic setting produced an IL-12-dependent antitumor response. Furthermore, triggering the T cell:DC crosstalk through non-canonical NF-κB agonism in combination with aPD1 treatment could potently enhance antitumor immunity. These data support an IL-12-driven "licensing" model of aPD-1 therapy, in which aPD-1 mAb targeting of T cells leads to tumor elimination only after successful crosstalk between these T cells and DCs. We suggest further that responses to immunotherapy can be improved through rational drug combinations that accentuate the crosstalk between lymphoid and myeloid immune compartments.

Real-time *in vivo* imaging allows one to identify not only primary targets of immunotherapeutics (drug pharmacokinetics) (Arlauckas et al., 2017) but also how the tumor microenvironment responds to treatment (drug pharmacodynamics). Consequently, this type of imaging complements the use of gene-deficient mouse models to study cancer treatments: whereas gene-deficient models can establish the relevance of particular genes in immunotherapy, imaging provides molecular dynamics at single-cell and spatial resolutions and over a longitudinal course of therapeutic response. Caveats still exist with this imaging approach, however, as distribution and effector functions of antibodies may differ between species and antibody compositions. It is also worth noting that the investigations presented in this study used cytokine reporter animals for readout of immune cells' functional attributes, as opposed to immune cells' identities. We believe this is important because antitumor immune functions may not necessarily be cell type dependent, so in theory different cell types can be imaged but the functional readout still remains. For example, in the experimental setups used in this study, we found that $CD8^+$ T cells and DCs are the primary producers of IFN-γ and IL-12, respectively; however, under different experimental contexts it is possible that NK cells may also produce IFN-γ and macrophages may also produce IL-12. It should also be noted that the present report focuses on pharmacodynamic imaging of aPD-1 and aCD40, although our imaging platform can in principle be used to interrogate any immune drug or other therapeutic agent, and further be expanded to additional functional readouts.

There is increasing support for DCs taking a center stage in checkpoint immunotherapies in cancer. In particular, the cDC1 subtype of DCs, which resembles the DC1 subtype presented here, is adept at cross-presenting antigens (Schlitzer and Ginhoux, 2014) and appears essential for T cell-driven antitumor immunity (Hildner et al., 2008). Interestingly, these DCs may be involved at different stages during the tumor rejection process: besides their critical role for priming T cells in lymph nodes (Martín-Fontecha et al., 2003), recent studies demonstrated that DCs can be found in tumors, where they recruit T cells and stimulate tumor-reactive T cell responses locally (Spranger et al., 2014; de Mingo Pulido et al., 2018). The findings presented here align with the notion that intratumoral DCs can exhibit key antitumor functions and promote aPD-1 immunotherapy. Systemic involvement of immunotherapy responses could also be relevant. For example, in the context of a longer duration of response, it is possible that aPD-1's antitumor activity is promoted initially by intratumoral DCs and T cells, and later by an additional pool of cells that are recruited from outside the tumor microenvironment (perhaps from the bone marrow or even from tumor-draining lymph nodes).

We found that $IL\text{-}12^+$ DCs do not always express the marker CD103 (encoded by *Itgae*), which is often used to define antitumor DCs. It is possible that CD103 is not required for DCs' antitumor functions and that its expression depends at least in part on the tissue where the DCs reside. In contrast, IL-12 may be both a marker and functional feature of immunostimulatory tumor DCs, based on our findings that (1) $IL\text{-}12^+$ DCs share many features with cross-presenting DC1 cells, including expression of *Batf3*, *Irf8*, *Flt3*, and *Ly75* (DEC205), and (2) IL-12 is required for immunotherapy efficacy. This notion further accords with prior evidence that cross-presenting tumor DCs have elevated IL-12 expression (Broz et al., 2014; Ruffell et al., 2014). Our data further indicate that IL-12-producing DCs can be generated by circulating precursors, although future studies should aim to precisely determine the ontogeny of these cells.

The findings presented here show that IL-12 cytokine signals supplied by intratumoral DCs assist antitumor immunity. It will be interesting to further investigate the interactions between $IL\text{-}12^+$ DCs, $IFN\text{-}\gamma^+$ T cells, and immunotherapeutics. For example, considering that DCs can express PD-L1 and that PD-1 is activated upon binding to PD-L1, it should be helpful to elucidate the function and fate of PD-L1 expressed by intratumoral DCs after aPD(L)1 treatment. Also, since $IL\text{-}12^+$ DCs express the highest levels of CD28's co-stimulatory ligands, CD80 and CD86, it is possible that these ligands contribute to an aPD-(L)1 antitumor response. Furthermore, IL-12 produced by intratumoral DCs may mediate antitumor effects through regulation of transcription factors such as T-bet and Eomes in effector T cells. Indeed, IL-12 may activate T-bet (Joshi et al., 2007; Szabo et al., 2000) and in doing so subvert exhaustion phenotypes (Kao et al., 2011). IL-12 may also repress Eomes (Takemoto et al., 2006), which is a major regulator of T cell exhaustion (Paley et al., 2012). Further study of cells responding to IL-12 could define additional avenues to reverse T cell exhaustion and potentiate antitumor immunity.

By looking at direct versus indirect effects of immunotherapy in the tumor microenvironment, we can start to better understand the mechanisms of tumor rejection *in vivo*, and, by extension, to rationally design combination therapeutic strategies. Here, we initially used the MC38 mouse tumor model because it is sensitive to aPD-1 treatment and thus is relevant to define mechanisms dictating treatment success. Furthermore, recapitulation of IFN-γ/IL-12-positive feedback mechanisms, through combination therapy, enables tumor control in harder-to-treat cancer models. Specifically, our analysis demonstrated that activating the non-canonical NF-κB pathway in intratumoral DCs through either CD40 agonism or cIAP inhibition can potently enhance aPD-1-mediated tumor control.

Treatments combining CD40 agonists with PD-1 pathway inhibitors (Clinicaltrials.gov: NCT03123783, NCT02376699) and cIAP inhibitors with aPD-L1 (Clinicaltrials.gov: NCT03270176) are currently in clinical trials. We suggest that both treatment strategies may rely upon the non-canonical NF-κB pathway

and DCs. Further, since our studies indicated that non-canonical NF-κB-targeting drugs depend upon IL-12 for mediating antitumor activity, we speculate that introduction of IL-12 could potently enhance aPD-1 immunotherapy. Previous attempts to develop IL-12-based therapies for human use had severely toxic consequences (Lasek et al., 2014) likely due to systemic administration routes. However, targeted intratumoral delivery of IL-12-encoding plasmids is safe and has already demonstrated antitumor efficacy as monotherapy (Daud et al., 2008). We suggest that further clinical studies should test whether rationally designed therapeutic strategies that accentuate T cell:DC cross-talk can enforce tumor-eliminating positive feedback mechanisms and expand the proportion of cancers sensitive to immunotherapy.

STAR★METHODS

Detailed methods are provided in the online version of this paper and include the following:

- KEY RESOURCES TABLE
- CONTACT FOR REAGENT AND RESOURCE SHARING
- EXPERIMENTAL MODEL AND SUBJECT DETAILS
  - Mice
  - Human Samples
  - Tumor Models
- METHOD DETAILS
  - Immunotherapy Treatment and Cytokine Modulation
  - Tumor Rechallenge
  - Bone Marrow Chimeras
  - Single Cell RNA Sequencing
  - Parabiosis
  - FTY 720 Treatments
  - Flow Cytometry – Mouse
  - Intravital Imaging
  - Isolation of Tumor-Infiltrating Lymphocytes and *in vitro* Restimulation
  - Tissue Isolation and Quantitative PCR
  - Human Studies
- QUANTIFICATION AND STATISTICAL ANALYSIS
  - Image Processing
  - Statistical analysis
- DATA AND SOFTWARE AVAILABILITY

SUPPLEMENTAL INFORMATION

Supplemental information includes seven figures and two videos and can be found with this article at https://doi.org/10.1016/j.immuni.2018.09.024.

ACKNOWLEDGMENTS

We thank S. Agarwala, K. Lewis, and S. Bhatia for contributing to the ImmunoPulse IL-12 studies; K. King, A. Klein, and C. Weinreb for assistance with single-cell analysis; S. He and C. Chan for help with bone marrow chimera experiments; and the Harvard Biopolymers Core for help with single cell library generation. This work was supported in part by the Samana Cay MGH Research Scholar Fund, the Robert Wenner Award from the Swiss Cancer League, and NIH grants R01-AI084880, R01-CA218579, and R01-AI123349 (to M.J.P.), NIH grant R01-CA206890 (to M.J.P. and R.W.), NIH grants R33-CA202064 and U01CA206997 (to R.W.), NIH grants P01 AI056299 and P50CA101942 (to G.J.F.), and Swiss National Cancer Foundation grant 320030_162575 (to A.Z.). C.S.G. was supported by NIH grant F31-CA196035; S.P.A. and S.G. were supported by NIH grant T32-CA79443; and C. Pfirschke was supported by the MGH ECOR Tosteson Postdoctoral Fellowship.

AUTHOR CONTRIBUTIONS

C.S.G. and S.P.A. designed the study, performed experiments, analyzed data, and wrote the manuscript. R.H.K., M.P.T., S.G., C. Piot, C.E., C. Pfirschke, M.S., J.G., S.E.W., S.O., E.B., R.H.P., and M.H.L. performed experiments and generated and analyzed data. G.J.F., S.I.P., C.G.T., A.P.A., A.I.D., A.Z., and R.W. provided input for research design and interpretation and edited the manuscript. M.J.P. directed the study and wrote the manuscript.

DECLARATION OF INTERESTS

M.J.P. has served as a consultant for Baxalta, Deciphera Pharmaceuticals, FORMA Therapeutics, Incyte Pharmaceuticals, Jounce Therapeutics, KSQ Therapeutics, Secarna, Siamab, and Syndax; these commercial relationships are unrelated to the current study. G.J.F. has patents/pending royalties on the PD-1 pathway from Roche, Merck, BMS, EMD-Serono, Boehringer-Ingelheim, AstraZeneca, Dako, and Novartis; he has also served on advisory boards for Roche, BMS, Xios, and Origimed. S.E.W. and S.O. are employees and stockholders in NanoString Technologies. E.B. and C.G.T. are employees and shareholders of OncoSec Inc. R.H.P., M.H.L., and A.P.A. have stock options in OncoSec Inc. A.P.A. has served as a consultant for OncoSec Inc and Valitor Bio and has research funding from Merck, BMS, AstraZeneca, MedImmune, Acerta, Incyte, Genentech, Idera, Dynavax, Tessa, Plexxicon, Checkmate, Regeneron, Novartis, and Amgen. A.I.D. has consulted for OncoSec Inc, Merck, and BMS. A.Z. has received research funding from Roche. R.W. is a cofounder of T2 Biosystems, Lumicell, Accure Health, and VisEn Medical (acquired by Perkin Elmer) and advises Moderna, Alivio Therapeutics, Tarveda Therapeutics, and BioAnalytix; these relationships are unrelated to the current study.

Received: April 13, 2018
Revised: July 30, 2018
Accepted: September 27, 2018
Published: December 11, 2018

SUPPORTING CITATIONS

The following reference appears in the Supplemental Information: Yan et al. (2018).

REFERENCES

Alloatti, A., Rookhuizen, D.C., Joannas, L., Carpier, J.M., Iborra, S., Magalhaes, J.G., Yatim, N., Kozik, P., Sancho, D., Albert, M.L., and Amigorena, S. (2017). Critical role for Sec22b-dependent antigen cross-presentation in antitumor immunity. J. Exp. Med. *214*, 2231–2241.

Arlauckas, S.P., Garris, C.S., Kohler, R.H., Kitaoka, M., Cuccarese, M.F., Yang, K.S., Miller, M.A., Carlson, J.C., Freeman, G.J., Anthony, R.M., et al. (2017). In vivo imaging reveals a tumor-associated macrophage-mediated resistance pathway in anti-PD-1 therapy. Sci. Transl. Med. *9*, 9.

Ayers, M., Lunceford, J., Nebozhyn, M., Murphy, E., Loboda, A., Kaufman, D.R., Albright, A., Cheng, J.D., Kang, S.P., Shankaran, V., et al. (2017). IFN-γ-related mRNA profile predicts clinical response to PD-1 blockade. J. Clin. Invest. *127*, 2930–2940.

Beatty, G.L., Chiorean, E.G., Fishman, M.P., Saboury, B., Teitelbaum, U.R., Sun, W., Huhn, R.D., Song, W., Li, D., Sharp, L.L., et al. (2011). CD40 agonists alter tumor stroma and show efficacy against pancreatic carcinoma in mice and humans. Science *331*, 1612–1616.

Broz, M.L., Binnewies, M., Boldajipour, B., Nelson, A.E., Pollack, J.L., Erle, D.J., Barczak, A., Rosenblum, M.D., Daud, A., Barber, D.L., et al. (2014). Dissecting the tumor myeloid compartment reveals rare activating antigen-presenting cells critical for T cell immunity. Cancer Cell *26*, 638–652.

Byrne, K.T., and Vonderheide, R.H. (2016). CD40 stimulation obviates innate sensors and drives T cell immunity in cancer. Cell Rep. *15*, 2719–2732.

Cella, M., Scheidegger, D., Palmer-Lehmann, K., Lane, P., Lanzavecchia, A., and Alber, G. (1996). Ligation of CD40 on dendritic cells triggers production of high levels of interleukin-12 and enhances T cell stimulatory capacity: T-T help via APC activation. J. Exp. Med. *184*, 747–752.

Dahan, R., Sega, E., Engelhardt, J., Selby, M., Korman, A.J., and Ravetch, J.V. (2015). FcγRs modulate the anti-tumor activity of antibodies targeting the PD-1/PD-L1 axis. Cancer Cell *28*, 285–295.

Daud, A.I., DeConti, R.C., Andrews, S., Urbas, P., Riker, A.I., Sondak, V.K., Munster, P.N., Sullivan, D.M., Ugen, K.E., Messina, J.L., and Heller, R. (2008). Phase I trial of interleukin-12 plasmid electroporation in patients with metastatic melanoma. J. Clin. Oncol. *26*, 5896–5903.

de Mingo Pulido, Á., Gardner, A., Hiebler, S., Soliman, H., Rugo, H.S., Krummel, M.F., Coussens, L.M., and Ruffell, B. (2018). TIM-3 regulates CD103+ dendritic cell function and response to chemotherapy in breast cancer. Cancer Cell *33*, 60–74.e6.

Engblom, C., Pfirschke, C., and Pittet, M.J. (2016). The role of myeloid cells in cancer therapies. Nat. Rev. Cancer *16*, 447–462.

Galon, J., Angell, H.K., Bedognetti, D., and Marincola, F.M. (2013). The continuum of cancer immunosurveillance: prognostic, predictive, and mechanistic signatures. Immunity *39*, 11–26.

Gordon, S.R., Maute, R.L., Dulken, B.W., Hutter, G., George, B.M., McCracken, M.N., Gupta, R., Tsai, J.M., Sinha, R., Corey, D., et al. (2017). PD-1 expression by tumour-associated macrophages inhibits phagocytosis and tumour immunity. Nature *545*, 495–499.

Hennessy, E.J., Adam, A., Aquila, B.M., Castriotta, L.M., Cook, D., Hattersley, M., Hird, A.W., Huntington, C., Kamhi, V.M., Laing, N.M., et al. (2013). Discovery of a novel class of dimeric Smac mimetics as potent IAP antagonists resulting in a clinical candidate for the treatment of cancer (AZD5582). J. Med. Chem. *56*, 9897–9919.

Hildner, K., Edelson, B.T., Purtha, W.E., Diamond, M., Matsushita, H., Kohyama, M., Calderon, B., Schraml, B.U., Unanue, E.R., Diamond, M.S., et al. (2008). Batf3 deficiency reveals a critical role for CD8alpha+ dendritic cells in cytotoxic T cell immunity. Science *322*, 1097–1100.

Hoves, S., Ooi, C.-H., Wolter, C., Sade, H., Bissinger, S., Schmittnaegel, M., Ast, O., Giusti, A.M., Wartha, K., Runza, V., et al. (2018). Rapid activation of tumor-associated macrophages boosts preexisting tumor immunity. J. Exp. Med. *215*, 859–876.

Huang, A.C., Postow, M.A., Orlowski, R.J., Mick, R., Bengsch, B., Manne, S., Xu, W., Harmon, S., Giles, J.R., Wenz, B., et al. (2017). T-cell invigoration to tumour burden ratio associated with anti-PD-1 response. Nature *545*, 60–65.

Hui, E., Cheung, J., Zhu, J., Su, X., Taylor, M.J., Wallweber, H.A., Sasmal, D.K., Huang, J., Kim, J.M., Mellman, I., and Vale, R.D. (2017). T cell costimulatory receptor CD28 is a primary target for PD-1-mediated inhibition. Science *355*, 1428–1433.

Joshi, N.S., Cui, W., Chandele, A., Lee, H.K., Urso, D.R., Hagman, J., Gapin, L., and Kaech, S.M. (2007). Inflammation directs memory precursor and short-lived effector CD8(+) T cell fates via the graded expression of T-bet transcription factor. Immunity *27*, 281–295.

Kamphorst, A.O., Wieland, A., Nasti, T., Yang, S., Zhang, R., Barber, D.L., Konieczny, B.T., Daugherty, C.Z., Koenig, L., Yu, K., et al. (2017). Rescue of exhausted CD8 T cells by PD-1-targeted therapies is CD28-dependent. Science *355*, 1423–1427.

Kao, C., Oestreich, K.J., Paley, M.A., Crawford, A., Angelosanto, J.M., Ali, M.A., Intlekofer, A.M., Boss, J.M., Reiner, S.L., Weinmann, A.S., and Wherry, E.J. (2011). Transcription factor T-bet represses expression of the inhibitory receptor PD-1 and sustains virus-specific CD8+ T cell responses during chronic infection. Nat. Immunol. *12*, 663–671.

Katakam, A.K., Brightbill, H., Franci, C., Kung, C., Nunez, V., Jones, C., 3rd, Peng, I., Jeet, S., Wu, L.C., Mellman, I., et al. (2015). Dendritic cells require NIK for CD40-dependent cross-priming of CD8+ T cells. Proc. Natl. Acad. Sci. USA *112*, 14664–14669.

Keir, M.E., Butte, M.J., Freeman, G.J., and Sharpe, A.H. (2008). PD-1 and its ligands in tolerance and immunity. Annu. Rev. Immunol. *26*, 677–704.

Lasek, W., Zagożdżon, R., and Jakobisiak, M. (2014). Interleukin 12: still a promising candidate for tumor immunotherapy? Cancer Immunol. Immunother. *63*, 419–435.

Lee, S.H., Carrero, J.A., Uppaluri, R., White, J.M., Archambault, J.M., Lai, K.S., Chan, S.R., Sheehan, K.C., Unanue, E.R., and Schreiber, R.D. (2013). Identifying the initiating events of anti-Listeria responses using mice with conditional loss of IFN-γ receptor subunit 1 (IFNGR1). J. Immunol. *191*, 4223–4234.

Lind, E.F., Ahonen, C.L., Wasiuk, A., Kosaka, Y., Becher, B., Bennett, K.A., and Noelle, R.J. (2008). Dendritic cells require the NF-kappaB2 pathway for cross-presentation of soluble antigens. J. Immunol. *181*, 354–363.

Ma, X., Chow, J.M., Gri, G., Carra, G., Gerosa, F., Wolf, S.F., Dzialo, R., and Trinchieri, G. (1996). The interleukin 12 p40 gene promoter is primed by interferon gamma in monocytic cells. J. Exp. Med. *183*, 147–157.

Macosko, E.Z., Basu, A., Satija, R., Nemesh, J., Shekhar, K., Goldman, M., Tirosh, I., Bialas, A.R., Kamitaki, N., Martersteck, E.M., et al. (2015). Highly parallel genome-wide expression profiling of individual cells using nanoliter droplets. Cell *161*, 1202–1214.

MartIn-Fontecha, A., Sebastiani, S., Höpken, U.E., Uguccioni, M., Lipp, M., Lanzavecchia, A., and Sallusto, F. (2003). Regulation of dendritic cell migration to the draining lymph node: impact on T lymphocyte traffic and priming. J. Exp. Med. *198*, 615–621.

Marty, R., Kaabinejadian, S., Rossell, D., Slifker, M.J., van de Haar, J., Engin, H.B., de Prisco, N., Ideker, T., Hildebrand, W.H., Font-Burgada, J., and Carter, H. (2017). MHC-I genotype restricts the oncogenic mutational landscape. Cell *171*, 1272–1283.e15.

Matson, V., Fessler, J., Bao, R., Chongsuwat, T., Zha, Y., Alegre, M.L., Luke, J.J., and Gajewski, T.F. (2018). The commensal microbiome is associated with anti-PD-1 efficacy in metastatic melanoma patients. Science *359*, 104–108.

McGranahan, N., Rosenthal, R., Hiley, C.T., Rowan, A.J., Watkins, T.B.K., Wilson, G.A., Birkbak, N.J., Veeriah, S., Van Loo, P., Herrero, J., and Swanton, C.; TRACERx Consortium (2017). Allele-specific HLA loss and immune escape in lung cancer evolution. Cell *171*, 1259–1271.e11.

Meredith, M.M., Liu, K., Darrasse-Jeze, G., Kamphorst, A.O., Schreiber, H.A., Guermonprez, P., Idoyaga, J., Cheong, C., Yao, K.H., Niec, R.E., and Nussenzweig, M.C. (2012). Expression of the zinc finger transcription factor zDC (Zbtb46, Btbd4) defines the classical dendritic cell lineage. J. Exp. Med. *209*, 1153–1165.

Nastala, C.L., Edington, H.D., McKinney, T.G., Tahara, H., Nalesnik, M.A., Brunda, M.J., Gately, M.K., Wolf, S.F., Schreiber, R.D., Storkus, W.J., et al. (1994). Recombinant IL-12 administration induces tumor regression in association with IFN-gamma production. J. Immunol. *153*, 1697–1706.

Ngiow, S.F., Young, A., Blake, S.J., Hill, G.R., Yagita, H., Teng, M.W., Korman, A.J., and Smyth, M.J. (2016). Agonistic CD40 mAb-driven IL12 reverses resistance to anti-PD1 in a T-cell-rich tumor. Cancer Res. *76*, 6266–6277.

Nirschl, C.J., Suárez-Fariñas, M., Izar, B., Prakadan, S., Dannenfelser, R., Tirosh, I., Liu, Y., Zhu, Q., Devi, K.S.P., Carroll, S.L., et al. (2017). IFNγ-dependent tissue-immune homeostasis is co-opted in the tumor microenvironment. Cell *170*, 127–141.e15.

Paley, M.A., Kroy, D.C., Odorizzi, P.M., Johnnidis, J.B., Dolfi, D.V., Barnett, B.E., Bikoff, E.K., Robertson, E.J., Lauer, G.M., Reiner, S.L., and Wherry, E.J. (2012). Progenitor and terminal subsets of CD8+ T cells cooperate to contain chronic viral infection. Science *338*, 1220–1225.

Pittet, M.J., Garris, C.S., Arlauckas, S.P., and Weissleder, R. (2018). Recording the wild lives of immune cells. Sci. Immunol. *3*, 3.

Reinhardt, R.L., Hong, S., Kang, S.-J., Wang, Z.E., and Locksley, R.M. (2006). Visualization of IL-12/23p40 in vivo reveals immunostimulatory dendritic cell migrants that promote Th1 differentiation. J. Immunol. *177*, 1618–1627.

Reinhardt, R.L., Liang, H.-E., Bao, K., Price, A.E., Mohrs, M., Kelly, B.L., and Locksley, R.M. (2015). A novel model for IFN-γ-mediated autoinflammatory syndromes. J. Immunol. *194*, 2358–2368.

Riaz, N., Havel, J.J., Makarov, V., Desrichard, A., Urba, W.J., Sims, J.S., Hodi, F.S., Martín-Algarra, S., Mandal, R., Sharfman, W.H., et al. (2017). Tumor and

microenvironment evolution during immunotherapy with nivolumab. Cell *171*, 934–949.e16.

Rizvi, N.A., Hellmann, M.D., Snyder, A., Kvistborg, P., Makarov, V., Havel, J.J., Lee, W., Yuan, J., Wong, P., Ho, T.S., et al. (2015). Cancer immunology. Mutational landscape determines sensitivity to PD-1 blockade in non-small cell lung cancer. Science *348*, 124–128.

Rooney, M.S., Shukla, S.A., Wu, C.J., Getz, G., and Hacohen, N. (2015). Molecular and genetic properties of tumors associated with local immune cytolytic activity. Cell *160*, 48–61.

Routy, B., Le Chatelier, E., Derosa, L., Duong, C.P.M., Alou, M.T., Daillère, R., Fluckiger, A., Messaoudene, M., Rauber, C., Roberti, M.P., et al. (2018). Gut microbiome influences efficacy of PD-1-based immunotherapy against epithelial tumors. Science *359*, 91–97.

Ruffell, B., Chang-Strachan, D., Chan, V., Rosenbusch, A., Ho, C.M., Pryer, N., Daniel, D., Hwang, E.S., Rugo, H.S., and Coussens, L.M. (2014). Macrophage IL-10 blocks CD8+ T cell-dependent responses to chemotherapy by suppressing IL-12 expression in intratumoral dendritic cells. Cancer Cell *26*, 623–637.

Salmon, H., Idoyaga, J., Rahman, A., Leboeuf, M., Remark, R., Jordan, S., Casanova-Acebes, M., Khudoynazarova, M., Agudo, J., Tung, N., et al. (2016). Expansion and activation of CD103(+) dendritic cell progenitors at the tumor site enhances tumor responses to therapeutic PD-L1 and BRAF inhibition. Immunity *44*, 924–938.

Satija, R., Farrell, J.A., Gennert, D., Schier, A.F., and Regev, A. (2015). Spatial reconstruction of single-cell gene expression data. Nat. Biotechnol. *33*, 495–502.

Schlitzer, A., and Ginhoux, F. (2014). Organization of the mouse and human DC network. Curr. Opin. Immunol. *26*, 90–99.

Schreiber, R.D., Old, L.J., and Smyth, M.J. (2011). Cancer immunoediting: integrating immunity's roles in cancer suppression and promotion. Science *331*, 1565–1570.

Slifka, M.K., Rodriguez, F., and Whitton, J.L. (1999). Rapid on/off cycling of cytokine production by virus-specific CD8+ T cells. Nature *401*, 76–79.

Spranger, S., Koblish, H.K., Horton, B., Scherle, P.A., Newton, R., and Gajewski, T.F. (2014). Mechanism of tumor rejection with doublets of CTLA-4, PD-1/PD-L1, or IDO blockade involves restored IL-2 production and proliferation of CD8(+) T cells directly within the tumor microenvironment. J. Immunother. Cancer *2*, 3.

Spranger, S., Bao, R., and Gajewski, T.F. (2015). Melanoma-intrinsic β-catenin signalling prevents anti-tumour immunity. Nature *523*, 231–235.

Szabo, S.J., Kim, S.T., Costa, G.L., Zhang, X., Fathman, C.G., and Glimcher, L.H. (2000). A novel transcription factor, T-bet, directs Th1 lineage commitment. Cell *100*, 655–669.

Takemoto, N., Intlekofer, A.M., Northrup, J.T., Wherry, E.J., and Reiner, S.L. (2006). Cutting Edge: IL-12 inversely regulates T-bet and eomesodermin expression during pathogen-induced CD8+ T cell differentiation. J. Immunol. *177*, 7515–7519.

Thurber, G.M., Yang, K.S., Reiner, T., Kohler, R.H., Sorger, P., Mitchison, T., and Weissleder, R. (2013). Single-cell and subcellular pharmacokinetic imaging allows insight into drug action in vivo. Nat. Commun. *4*, 1504.

Topalian, S.L., Hodi, F.S., Brahmer, J.R., Gettinger, S.N., Smith, D.C., McDermott, D.F., Powderly, J.D., Carvajal, R.D., Sosman, J.A., Atkins, M.B., et al. (2012). Safety, activity, and immune correlates of anti-PD-1 antibody in cancer. N. Engl. J. Med. *366*, 2443–2454.

Weinreb, C., Wolock, S., and Klein, A.M. (2018). SPRING: a kinetic interface for visualizing high dimensional single-cell expression data. Bioinformatics *34*, 1246–1248.

Weissleder, R., Nahrendorf, M., and Pittet, M.J. (2014). Imaging macrophages with nanoparticles. Nat. Mater. *13*, 125–138.

Wherry, E.J. (2011). T cell exhaustion. Nat. Immunol. *12*, 492–499.

Yan, J., Smyth, M.J., and Teng, M.W.L. (2018). Interleukin (IL)-12 and IL-23 and their conflicting roles in cancer. Cold Spring Harb. Perspect. Biol. *10*, 10.

STAR★METHODS

KEY RESOURCES TABLE

REAGENT or RESOURCE	SOURCE	IDENTIFIER
Antibodies		
Anti-Mouse PD-1 (clone 29F.1A12)	Gordon J. Freeman	N/A
Anti-Mouse CD40 (clone FGK4.5)	Bio X Cell	Cat# BE0016-2, RRID:AB_1107647
Rat IgG2a Isotype Control Antibody	Bio X Cell	Cat# BE0089, RRID:AB_1107769
Anti-Mouse IL-12p40 (clone C17.8)	Bio X Cell	Cat# BE0051, RRID:AB_1107698
Anti-Mouse IFN-γ (clone XMG1.2)	Bio X Cell	Cat# BE0055; RRID:AB_1107694
Anti-Mouse CD8α (clone 53-6.7)	Bio X Cell	Cat# BE0004-1; RRID:AB_1107671
Anti-Mouse CD3ε (clone 145-2C11)	Thermo Fisher Scientific	Cat# 14-0031-81, RRID:AB_467048
Anti-Mouse CD28 (clone 37.51)	Thermo Fisher Scientific	Cat# 16-0281-85, RRID:AB_468922
Anti-Mouse/Human CD11b (clone M1/70)	BioLegend	Cat# 101237, RRID:AB_11126744
Anti-Mouse CD8α (clone 53-6.7)	BioLegend	Cat# 100729, RRID:AB_493702
Anti-Mouse CD45 (clone 30-F11)	BD Biosciences	Cat# 557659, RRID:AB_396774
Anti-Mouse F4/80 (clone BM8)	BioLegend	Cat# 123115, RRID:AB_893493
Anti-Mouse CD11c (clone N418)	BioLegend	Cat# 117349, RRID:AB_2563905
Anti-Mouse MHC II I-A/I-E (clone M5/114.15.2)	BioLegend	Cat# 107608, RRID:AB_313323
Anti-Mouse CD103 (clone 2E7)	BioLegend	Cat# 121422, RRID:AB_2562901
Anti-Mouse IFN-γ (clone XMG1.2)	BioLegend	Cat# 505825, RRID:AB_1595591
TruStain fcX Anti-Mouse CD16/32 (clone 93)	BioLegend	Cat# 101319, RRID:AB_1574973
Anti-Mouse CD90.2 (clone 53-2.1)	BD Biosciences	Cat# 553006, RRID:AB_394545
Anti-Mouse CD45.1 (clone A20)	Thermo Fisher Scientific	Cat# 25-0453-81, RRID:AB_469628
Anti-Mouse CD45.2 (clone 104)	BioLegend	Cat# 109831, RRID:AB_10900256
Ultra LEAF Purified anti-Human CD3 (clone OKT3)	BioLegend	BioLegend Cat# 317348, RRID:AB_2571995
Anti-Human CD3 (clone SK7)	Thermo Fisher Scientific	Cat# 12-0036-41, RRID:AB_10804272
Anti-Human CD4 (clone SK3)	BD Biosciences	Cat# 651849
Anti-Human CD8 (clone SK1)	Thermo Fisher Scientific	Cat# 11-0087-42, RRID:AB_10557240
Anti-Human CD11b (clone ICRF44)	Thermo Fisher Scientific	Cat# 46-0118-42, RRID:AB_10597890
Anti-Human CD14 (clone HCD14)	BioLegend	Cat# 325631, RRID:AB_2563327
Anti-Human CD11c (clone 3.9)	Thermo Fisher Scientific	Cat# 46-0116-42, RRID:AB_10596368
Anti-Human CD19 (clone SJ25C1)	BioLegend	Cat# 363015, RRID:AB_2564206
Anti-Human CD45 (clone 2D1)	BD Biosciences	Cat# 560178, RRID:AB_1645479
Anti-Human CD56 (clone AF12-7H3)	Miltenyi	Cat# 130-090-843, RRID:AB_244332
Chemicals, Peptides, and Recombinant Proteins		
Recombinant Mouse Flt3L	Peprotech	Cat# 550704
Recombinant Mouse IFN-γ	Peprotech	Cat# 315-05
Recombinant Mouse IL-12p70	Peprotech	Cat# 210-12
7-Aminoactinomycin D	Sigma	Cat# A9400-1MG
Collagenase II	Worthington	Cat# LS004177
Ferumoxytol	AMAG Pharmaceuticals	N/A
500 kDa Amino Dextran	Thermo Fisher Scientific	Cat# D7144
AZD5582	Selleck Chemical	Cat# S7362
FTY720	Cayman Chemical	Cat# 10006292

(*Continued on next page*)

Continued

REAGENT or RESOURCE	SOURCE	IDENTIFIER
Diphtheria Toxin	Sigma-Aldrich	Cat# D0564-1MG
BD GolgiPlug	BD Biosciences	Cat# 555029
Collagenase IV	Worthington	Cat# LS004186
Hyaluronidase	Sigma-Aldrich	Cat# H3506
DNase I, Type IV	Sigma-Aldrich	Cat# D5025
Accutase	PAA Laboratories GmbH	Cat# L11-007
Recombinant Human IL-12p70	Peprotech	Cat# 200-12
Biological Samples		
Human Tumor Tissue: Lung Adenocarcinoma	University Hospital Basel	N/A
Human Tumor Tissue: Squamous Cell Carcinoma	University Hospital Basel	N/A
Human Tumor Tissue: Synovial Sarcoma	University Hospital Basel	N/A
Human Tumor Tissue: Melanoma	UCSF Medical Center and Huntsman Cancer Institute	Clinical Trial: NCT01502293
Critical Commercial Assays		
CD8a+ T cell Isolation Kit, Mouse	Miltenyi Biotec	Cat# 130-104-075
Chromium Single Cell 3′ Reagent Kit	10X Genomics	Cat# 120267
SAIVI Alexa Fluor 647 Antibody/Protein Labeling Kit	Thermo Fisher Scientific	Cat# S30044
BD Cytofix/Cytoperm Kit	BD Biosciences	Cat# 554714
OptEIA Human IFN- γ ELISA Set	BD Biosciences	Cat# 555142
NanoString PanCancer IO360	NanoString Technologies	N/A
PAXgene Tissue Fixative	PreAnalytix	Cat# 765112
RecoverAll Total Nucleic Acid Isolation Kit	Thermo Fisher Scientific	Cat# AM1975
RNeasy RNA Isolation Mini Kit	QIAGEN	Cat# 74104
Deposited Data		
Raw Single Cell RNA Sequencing Data (Control)	NCBI Gene Expression Omnibus	GEO: GSM3090155
Raw Single Cell RNA Sequencing Data (aPD-1)	NCBI Gene Expression Omnibus	GEO: GSM3090156
Experimental Models: Cell Lines		
Cancer Cell Line: MC38	Mark J. Smyth	RRID:CVCL_B288
Cancer Cell Line: B16F10	ATCC	ATCC Cat# CRL-6475, RRID:CVCL_0159
Cancer Cell Line: MC38 H2B-mApple	Mikael Pittet and Ralph Weissleder	N/A
Experimental Models: Organisms/Strains		
Mouse: WT or CD45.2 C57BL/6J	The Jackson Laboratory	Stock# 000664 RRID:IMSR_JAX:000664
Mouse: B6.129-Il12b^{tm1Lky}/J	The Jackson Laboratory	Stock# 006412 RRID:IMSR_JAX:006412
Mouse: B6.129S4-Ifng$^{tm3.1Lky}$/J	The Jackson Laboratory	Stock#017581 RRID:IMSR_JAX:017581
Mouse: B6N.129-Map3k14^{tm1Rds}/J	The Jackson Laboratory	Stock# 025557 RRID:IMSR_JAX:025557
Mouse: B6(Cg)-Zbtb46$^{tm1(HBEGF)Mnz}$/J	The Jackson Laboratory	Stock# 019506 RRID:IMSR_JAX:019506
Mouse: C57BL/6J-Tg(Itgax-cre,-EGFP)4097Ach/J	The Jackson Laboratory	Stock# 007567 RRID:IMSR_JAX:007567
Mouse: C57BL/6N-Ifngr1$^{tm1.1Rds}$/J	The Jackson Laboratory	Stock# 025394 RRID:IMSR_JAX:025394
Mouse: CD45.3	David T. Scadden	N/A
Oligonucleotides		
Mouse IL-12b Taqman Probe	Thermo Fisher Scientific	Cat# 4331182 AssayID: Mm01288989_m1
Mouse HPRT Taqman Probe	Thermo Fisher Scientific	Cat# 4331182 AssayID: Mm01545399_m1

(*Continued on next page*)

Continued		
REAGENT or RESOURCE	SOURCE	IDENTIFIER
Software and Algorithms		
Seurat R Package	(Satija et al., 2015)	https://satijalab.org/seurat/; RRID: SCR_016341
FIJI ImageJ Version 1.51s	FIJI	https://fiji.sc; RRID: SCR_002285
SPRING	(Weinreb et al., 2017)	https://kleintools.hms.harvard.edu/tools/spring.html
FlowJo v.10.4	FlowJo, LLC	RRID: SCR_008520
Graphpad Prism v.7	GraphPad Prism	RRID: SCR_002798
DAVID Bioinformatics Resource 6.8	NIH	RRID: SCR_001881

CONTACT FOR REAGENT AND RESOURCE SHARING

Further information and requests for resources or reagents should be directed to the corresponding author and Lead Contact, Mikael J. Pittet (mpittet@mgh.harvard.edu).

EXPERIMENTAL MODEL AND SUBJECT DETAILS

Mice

All animals were bred and housed under specific pathogen free conditions at the Massachusetts General Hospital. Experiments were approved by the MGH Institutional Animal Care and Use Committee (IACUC) and were performed in accordance with MGH IACUC regulations. The following mouse strains were used in this study: Female C57BL6/J mice (8 - 12 week old) were purchased from Jackson Laboratories (Bar Harbor, ME). GREAT (IFN-γ-IRES-eYFP Cat #017581), IL-12p40-IRES-eYFP (Cat #006412), *CD11c-cre* (Cat #007567), *Ifngr1*$^{fl/fl}$ (Cat #025394), and *Zbtb46-DTR* (Cat# 025394) were obtained from Jackson Laboratories.

Human Samples

Fresh tumor specimens were obtained from 6 adult cancer patients undergoing tumor resections at University Hospital Basel, Switzerland. Tissues were used for *in vitro* re-stimulation and analysis. The study was approved by the local Ethical Review Board (Ethikkommission Nordwestschweiz) and University Hospital Basel, Switzerland. All patients consented in writing to the analysis of their tumor samples.

Patient	Gender	Health Status	Age
BS-661	M	Cancer	55
BS-728	M	Cancer	77
LA-061	N/A	Cancer	73
BS-705_T	M	Cancer	74
BS-698_T	F	Cancer	78
BS-469_T	M	Cancer	83

ImmunoPulse IL-12 treated tumor tissue samples were obtained from 19 melanoma patients from clinical trial NCT01502293. All biopsies were from University of California, San Francisco Medical Center-Mt. Zion, San Francisco, and Huntsman Cancer Institute, Salt Lake City, Utah, and were approved by each organization's institutional review board.

Patient	Gender	Disease Status	Age
1	M	Stage III c	66
2	M	Stage III b	88
3	M	Stage IV M1c	80
4	F	Stage III c	56
5	M	Stage IV M1a	65
6	F	Stage III b	89
7	M	Stage IV M1a	59
8	M	Stage III c	56
9	M	Stage III c	55
10	M	Stage IV M1a	63
11	M	Stage IV M1a	56
12	M	Stage IV M1a	44
13	M	Stage IV M1a	82
14	M	Stage IV M1b	74
15	M	Stage IV M1b	88
16	M	Stage IV M1c	58
17	M	Stage III c	61
18	M	Stage III c	59
19	M	Stage III b	65

Tumor Models

MC38 tumor cell lines were obtained from Dr. Mark Smyth (QIMR Berghofer). MC38 cells were implanted at 2×10^6 cells in the flank. B16F10 cell lines were obtained from ATCC. B16F10 cells were implanted intradermally at 0.5×10^6 cells in the flank. All tumor models were allowed to grow for one week prior to therapy. Tumor sizes were approximately 75 mm^3 before treatment initiation, and starting tumor volumes were normalized between treatment groups. Percent tumor changes were calculated as percent difference of mouse tumor volume from pre-treatment baseline, measured using digital caliper. Lung seeding B16F10 models received 0.5×10^6 cells intravenously and were allowed to grow for 10 days from the point of implantation. Mouse tumors were allowed to grow to a maximum of 2 cm in diameter, or until tumor ulceration occurred. These were considered as endpoints for survival experiments in accordance with MGH IACUC regulations.

METHOD DETAILS

Immunotherapy Treatment and Cytokine Modulation

Tumor bearing mice, with a tumor size of approximately 75 mm^3, were treated with 200 μg of aPD-1 and/or 100 μg of aCD40 intraperitoneally for immunotherapy studies. For combination treatment studies, both aPD-1 and aCD40 were administered at the same time. For IL-12 neutralization studies, mice were dosed with 500 μg of anti-IL-12p40 Clone 17.8 daily for 5-7 days following aPD-1 therapy. Neutralization of IFN-γ *in vivo* was performed by administering 1 mg of anti-IFN-γ Clone XMG1.2 initially with 500 μg of anti-IFN-γ dosed daily intraperitoneally for days 1-3. The cIAP1/2 inhibitor AZD5582 (Hennessy et al., 2013) was purchased from Selleck Chem and was resuspended in sterile saline. Mice received a single dose of AZD5582 at 10 mg/kg, intraperitoneally. For IL-12 supplementation studies, recombinant IL-12 (1 μg in 100 μL saline) was delivered peritumorally and intraperitoneally, half dose each, for 5 consecutive days when indicated.

Tumor Rechallenge

Long-term surviving mice from aPD-1 and aCD40 combination therapy were re-challenged with either MC38 or B16F10 tumors at 50 days following primary tumor rejection. MC38 and B16F10 re-challenge doses were 2×10^6 cells and 0.5×10^6 cells respectively in the contralateral flank. Naive C57BL/6J mice were implanted alongside re-challenge mice, and these mice were monitored for tumor growth for 2 weeks following implantation

Bone Marrow Chimeras

For bone marrow chimera studies, recipient C57BL/6J mice were irradiated (10 Gray dose) in one session, and mice were injected intravenously with 5×10^6 or 3×10^6 whole bone marrow cells from B6(Cg)-Zbtb46tm1(HBEGF)Mnz/J (*Zbtb46-DTR*) or B6N.129-Map3k14tm1Rds/J (NIK–/–) respectively. Control mice were irradiated and re-constituted with C57BL/6J whole bone marrow (5×10^6 cells). Mice were then left to reconstitute for 8 weeks before tumor growth experiments. Mice receiving diphtheria

toxin (DT) (Sigma-Aldrich) were dosed at 10 ng of DT per gram of body weight to initiate depletion and then maintained at 4 ng of DT per gram of body weight every 3 days following initial depletion.

Single Cell RNA Sequencing

MC38 tumors were implanted into the flanks of C57BL6/J mice and allowed to grow for 7 days before immunotherapy treatment. Mice were untreated or aPD-1 treated. Tumors were harvested 3 days after initiation of therapy. Tumors were digested using collagenase II (Worthington) and $CD45^+$ cells were sorted from single cell suspensions using a BD FACSAria sorter. Cells were manually counted with a hemocytometer and trypan blue viability stain, and 3132 cells from the control treated and 8178 cells from the aPD-1 treated tumors were recovered directly in PBS with 0.04% BSA (400 μg/ml) without centrifugation and kept on ice. Live cells were single cell sorted into GEMS (Gel Bead in EMulsion) using the 10X Genomics Chromium system provided by the HMS Biopolymers core. GEMS were processed and libraries were prepared according to the Chromium Single Cell 3′ Reagent Kit v2 User guide (10X Genomics). Library QC was done by the HMS Biopolymers core and the libraries were sequenced on an Illlumina NextSeq at an average of 29,000 reads per cell. In total, 4095 cells (1154 untreated and 2941 aPD-1 treated cells) passed QC and were sequenced. 10X Cell Ranger 2.1.0 software was used for generation of fastq files and gene-barcode matrices. Loupe Cell Browser 2.0.0 and the Seurat R package (Satija et al., 2015) and SPRING (Weinreb et al., 2018) were used for clustering and analysis. Gene ontology analysis was performed using the DAVID Bioinformatics Resource v.6.8.

Parabiosis

CD45.3 and B6.129-Il12btm1Lky/J (IL-12 reporter) mice were placed under anesthesia (2% isoflurane) shaved on their sides and elbows and knees were stitched together with a black monofilament nylon suture (Ethicon). Animals were provided with buprenorphine as an analgesic for 3 days following surgery. After a 3 week recovery period, both mice from the parabiotic pair were challenged with MC38 tumors on the outer flank. Tumors were allowed to grow for 7 days before treatment with aPD-1 immunotherapy, and tumors were harvested 2 days following immunotherapy to analyze IL-12 dendritic cell populations by flow cytometry.

FTY 720 Treatments

Mice were implanted with MC38 tumors in the flank and cohorts of mice were sorted into groups of similar tumor size before treatment initiation. Tumors were allowed to grow for 7 days before treatments. Mice were treated or not with 1.25 mg/kg of FTY720 (Cayman Chemical) i.p. 2 hours before aPD-1 treatment, and were maintained daily on 1.25 mg/kg FTY720 throughout the duration of the experiment. Blood from mice was used to confirm lymphocyte trafficking defects.

Flow Cytometry – Mouse

Tumor tissue or tumor draining lymph nodes were isolated from mice and minced using surgical scissors. Tissues were then digested using 0.2 mg/ml Collagenase II (Worthington) in RPMI 1640 media (CellGro) at 37°C for 30 minutes and then strained through a 40 μm filter (BD Falcon). Cell suspensions were incubated with Fc Block TruStain FcX Clone 93 (Biolegend) in PBS containing 0.5% BSA and 2 mM EDTA before staining with fluorochrome labeled antibodies. Antibodies against CD11b (M1/70, Biolegend), CD8a (53-6.7, Biolegend), CD45 (30-F11, BD), F4/80 (BM8, Biolegend), CD11c (N418, Biolegend), MHC II I-A/I-E (M5/114.15.2, Biolegend), CD103 (2E7, Biolegend), IFN-γ (XMG1.2, Biolegend) were used for marker staining. 7AAD viability staining was used to exclude dead cells from analysis. Samples were run on a LSR II flow cytometer and analyzed using FlowJo software (Treestar). For intracellular cytokine staining, samples were incubated for 5 hours with GolgiPlug (BD) at 1 μl per ml of culture media. Cells were then surface stained and then fixed and permeabilized using the BD Cytofix/Cytoperm kit (BD) according to manufacturer's protocol and stained for intracellular cytokines.

Intravital Imaging

Interferon gamma reporter (IFN-γ-eYFP) or IL-12p40 reporter (IL12p40-eYFP) mice were anesthetized and dorsal skin-fold window chambers were installed as previously described (Thurber et al., 2013) and mice were treated with analgesic (Buprenorphine 0.1 mg/kg/day) for 3 days following chamber implantation. Twenty-four hours after window implantation, MC38-H2B-mApple cells (2×10^6 in 20 μl) were injected in the fascia layer. Pacific Blue-dextran nanoparticle (containing 1 nmol Pacific Blue dye) was injected 1 week after tumor implantation for macrophage labeling. On the next day, Pacific Blue-dextran (containing 37 μg dextran and 56 nmol Pacific Blue dye) for vascular labeling was delivered via a 30-gauge catheter inserted in the tail vein of the anesthetized mouse (2% isoflurane in oxygen). Anesthetized mice were kept on a heating pad kept at 37°C, vital signs monitored and mice were imaged using an Olympus FluoView FV1000MPE confocal imaging system (Olympus America). A 2x air objective XL Fluor 2x/340 (NA 0.14; Olympus America) was used to select regions near tumor margins and tumor vasculature by an operator blinded to treatment conditions. Higher magnification Z stack images were acquired using a XLUMPLFL 20 × water immersion objective (NA 0.95; Olympus America) with 1.5x digital zoom. Sequential scanning (5 μm slices) with 405, 473, 559, and 635 nm lasers was performed using voltage and power settings that were optimized using fluorescence minus-one control mice prior to time lapse acquisition. DM405/473/559/635 nm dichroic beam splitters (SDM473, SDM560, and SDM 640) and emission filters (BA430-455, BA490-540, BA575-620, BA575-675) were sourced from Olympus America. For time lapse acquisitions, a total frame interval of 133 s was acquired at non-overlapping coordinates. For CD8+ cell depletions, 200 μg of aCD8 was delivered 24 hours prior to aPD-1. Unlabeled antibodies were used with the exception of specific cases where AF647-aPD-1 mAb or AF647-aCD40-mAb

were delivered for drug distribution studies. Fluorochrome labeled antibodies were delivered at the same dose as unlabeled antibodies.

Isolation of Tumor-Infiltrating Lymphocytes and *in vitro* Restimulation

MC38 tumors were digested into single cell suspensions similar to tissue processing for flow cytometry analysis and were passed through a 40 μm filter. Cells were then labeled using the Miltenyi CD8α T cells enrichment kit (Miltenyi Biotec) and isolated using magnetic sorting according to manufacturer's protocols. Tissue culture plates were coated with anti-CD3ε and anti-CD28 at a concentration of 10 μg/ml and 5 μg/ml respectively in PBS for 12 hours, and excess antibody was aspirated before T cell addition. IL-12 was added into culture media at a concentration of 20 ng/ml. Cells were stimulated for 72 hours before addition of GolgiPlug for 5 hours for intracellular cytokine staining

Tissue Isolation and Quantitative PCR

Fresh MC38 tumor tissue (20-30 mg) from WT C57BL6/J aPD-1 treated mice, WT C57BL6/J aPD-1/aIFN-γ treated mice, aPD-1 treated *Ifngr1*$^{fl/fl}$ mice, or aPD-1 treated *Cd11c-cre Ifngr1*$^{fl/fl}$ mice, were finely minced using surgical scissors and lysed in RLT lysis buffer (QIAGEN) and frozen. Samples were then thawed and RNA was extracted using the QIAGEN Mini RNA extraction kit, and reverse transcribed using the High-Capacity cDNA kit (Thermo Fisher Scientific). Quantitative PCR was performed using Il12p40 Taqman Gene Expression probes (Thermo Fisher Scientific) and referenced to HPRT expression using 10 ng of cDNA per sample. The ΔΔCT method was used to quantitate Il12p40 expression across samples.

Human Studies

We performed two human studies to address the following questions: the first study aimed to define whether IL-12 delivery into tumors can enhance antitumor T cell signatures *in vivo* (ImmunoPulse, tavokinogene telseplasmid, IL-12 studies); the second study assessed whether IL-12 can activate tumor-infiltrating CD8+ T cells directly (IL-12 *ex vivo* studies), as detailed below.

ImmunoPulse IL-12 studies: Tumor biopsies from 19 melanoma patients enrolled in an ongoing clinical trial (NCT01502293) were used to assess whether intratumoral treatment with ImmunoPulse IL-12, a plasmid electroporation method that delivers IL-12 directly to tumors (Daud et al., 2008), induced a cytolytic immune signature within tumors. Patients presented with stage IIIB, IIIC, or IV M1a melanoma and with at least one lesion ≥ 0.3 cm x 0.3 cm in longest perpendicular diameters that was accessible for electroporation; patients may have had prior chemotherapy or immunotherapy (excluding prior therapy with IL-12 or gene therapy) but must have stopped treatment at least 4 weeks prior to study enrollment. All biopsies were from University of California, San Francisco Medical Center-Mt. Zion, San Francisco, and Huntsman Cancer Institute, Salt Lake City, Utah. Skin tumor tissue was isolated at two time points: first on the day of screening and then either on week 4 (15 of 19 patients (78.9%)), 6 (3 of 19 patients (15.8%)) or 12 (1 of 19 patients (5.3%)) after treatment began. The same lesions were biopsied pre-treatment and post-treatment when possible, regardless of time point. If no matched post-treatment lesions were available, week 4 biopsies from unmatched lesions were used (12 of 19 lesions (63.2%) were matched, 7 of 19 lesions (36.8%) were unmatched). Biopsies were fixed in PAXgene tissue fixative (PreAnalytiX, Hombrechtikon, Switzerland) and embedded in paraffin at Cureline (Brisbane, CA). 8 × 10 micron tissue curls were used for RNA extraction via RecoverAllTM Total Nucleic Acid Isolation Kits (ThermoFisher Waltham, MA) according to manufacturer's protocol. If necessary, RNA was concentrated using RNA Clean & Concentrator-5 kits according to manufacturer's protocol (Zymo Research Irvine, CA). Up to 100 ng of RNA was run on NanoString's PanCancer IO360TM beta version (NanoString Technologies Seattle, WA). Analysis was completed using NanoString's nSolver analysis software 3.0 pack. Data were normalized to control genes. Data were excluded if binding density, positive controls, or normalization factors were outside of the acceptable ranges set by NanoString. Post-treatment signals from selected genes were normalized to matched pre-treatment sample signals and plotted as a fold change relative to pre-treatment gene expression data.

IL-12 *ex vivo* studies: Fresh tumor resections from six cancer patients undergoing surgical treatment at University Hospital Basel, Switzerland were used to assess whether IL-12 can directly activate human tumor-infiltrating CD8+ T cells upon isolation of these cells *ex vivo*. Tumor tissue (two lung adenocarcinomas, three squamous cell carcinomas and one synovial sarcoma) was collected from six different patients undergoing primary surgical treatment between November 2015 and November 2017. The study was approved by the local Ethical Review Board (Ethikkommission Nordwestschweiz) and all patients consented in writing to the analysis of their tumor samples. The solid tumor lesions were mechanically dissociated and enzymatically digested using accutase (PAA), collagenase IV (Worthington), hyaluronidase (Sigma) and DNase type IV (Sigma), directly after excision. Single cell suspensions were prepared and cryopreserved in liquid nitrogen in 90% fetal calf serum (FCS, Brunschwig Pan Biotech) and 10% dimethylsulfoxide (DMSO, Sigma) until further usage. Thawed tumor digests were stained with the appropriate fluorochrome-coupled antibodies in PBS with 2% FCS and sorted for CD8+ T cells by flow cytometry using a BD SorpAriaIII. Sorting purity was measured by reanalyzing the sorted cells and always reached > 95% purity. Cells were rested at 37°C, 5% CO2 in 96 well plates in supplemented RPMI medium (Sigma, supplemented with 10% heat-inactivated and tested FCS, 1 mM pyruvate, 2 mM glutamine, 1% penicillin and streptomycin, 1% non-essential amino acids) for 18 hours, and further stimulated with 10 ng/ml recombinant human IL-12p70 (PeproTech) and/or 0.5 μg/ml OKT3 anti-CD3 antibody (UltraLEAF Purified, Biolegend) in supplemented RPMI medium and incubated for 3 days at 37°C, 5% CO2. IFN-γ secreted by these cultures was then measured by enzyme-linked immunosorbent assay according to the instructions by the manufacturer (BD, OptEIA human IFN-γ ELISA set). The following anti-human mAbs were used: CD3 PE (clone SK7, eBioscience); CD4 BV711 (clone SK3, BD); CD8 FITC (clone SK1, eBioscience); CD11b PerCP eFluor710 (clone ICRF44,

eBioscience), CD11c PerCP eFluor710 (clone 3.9, eBioscience); CD14 PerCP-eFluor710 (clone 61D3, Biolegend); CD19 PerCP-Cy5.5 (clone SJ25C1, Biolegend); CD45 APC-H7 (clone 2D1, BD PharMingen); CD56 APC (clone AF12-7H3, Miltenyi).

QUANTIFICATION AND STATISTICAL ANALYSIS

Image Processing

Images were Z-projected, cropped, and de-speckled for clarity using FIJI running ImageJ version 2 (6). For quantification, raw Z stack images were processed using rolling ball background subtraction, Renyi Entropy thresholding, and cell counting macros run through customized Java scripts in the FIJI environment. TAM and tumor vessels were segmented by pixel size and shape exclusion parameters. Cell number divided by area were reported relative to baseline prior to treatment. The Manual Tracking Plugin was used in FIJI for cell tracking. The slope of the regression function fitted to the mean displacement plot for each cell calculated to derive the cell motility coefficients (M), according to the following formula: $M = d2 / 4t$, where d is displacement from origin at time t.

Statistical analysis

Flow and imaging data were collected using FlowJo Version 10.4 and the FIJI package of ImageJ running version 1.51 s. This and other primary data was collected and organized using Microsoft Excel (version 14.6.3). All statistical analyses were performed using Graphpad Prism Version 7. Mouse cohort sizes were pre-determined using power analyses, as reported previously(Arlauckas et al., 2017). Values reported in figures are expressed as the standard error of the mean, unless otherwise indicated. For normally-distributed datasets, we used 2-tailed Student's t test and one-way ANOVA followed by Bonferroni's multiple comparison test. When variables were not normally distributed, we performed non-parametric Mann-Whitney or Kuskal-Wallis tests. For survival analysis, p values were computed using the Log Rank test. p values > 0.05 were considered not significant (n.s.), p values < 0.05 were considered significant. * p value < 0.05, ** p value < 0.01, *** p value < 0.001, **** p value < 0.0001.

DATA AND SOFTWARE AVAILABILITY

Raw data for single cell RNA sequencing from sorted CD45+ cell populations from MC38 tumors can be found at the Gene Expression Omnibus Repository (GEO). The accession number for control (untreated) samples is GSM3090155. The accession number for aPD-1-treated samples is GSM3090156.

Immunity, Volume *49*

Supplemental Information

Successful Anti-PD-1 Cancer Immunotherapy Requires T Cell-Dendritic Cell Crosstalk Involving the Cytokines IFN-γ and IL-12

Christopher S. Garris, Sean P. Arlauckas, Rainer H. Kohler, Marcel P. Trefny, Seth Garren, Cécile Piot, Camilla Engblom, Christina Pfirschke, Marie Siwicki, Jeremy Gungabeesoon, Gordon J. Freeman, Sarah E. Warren, SuFey Ong, Erica Browning, Christopher G. Twitty, Robert H. Pierce, Mai H. Le, Alain P. Algazi, Adil I. Daud, Sara I. Pai, Alfred Zippelius, Ralph Weissleder, and Mikael J. Pittet

Supplementary Information

Successful anti-PD-1 Cancer Immunotherapy Requires T Cell-Dendritic Cell Crosstalk Involving the Cytokines IFN-γ and IL-12

Christopher S. Garris*, Sean P. Arlauckas*, Rainer Kohler, Marcel P. Trefny, Seth Garren, Cécile Piot, Camilla Engblom, Christina Pfirschke, Marie Siwicki, Jeremy Gungabeesoon, Gordon J. Freeman, Sarah E. Warren, SuFey Ong, Erica Browning, Christopher G. Twitty, Robert H. Pierce, Mai H. Le, Alain P. Algazi, Adil I. Daud, Sara I. Pai, Alfred Zippelius, Ralph Weissleder, Mikael J. Pittet#

*These authors contributed equally
#Corresponding author

Supplemental Figures

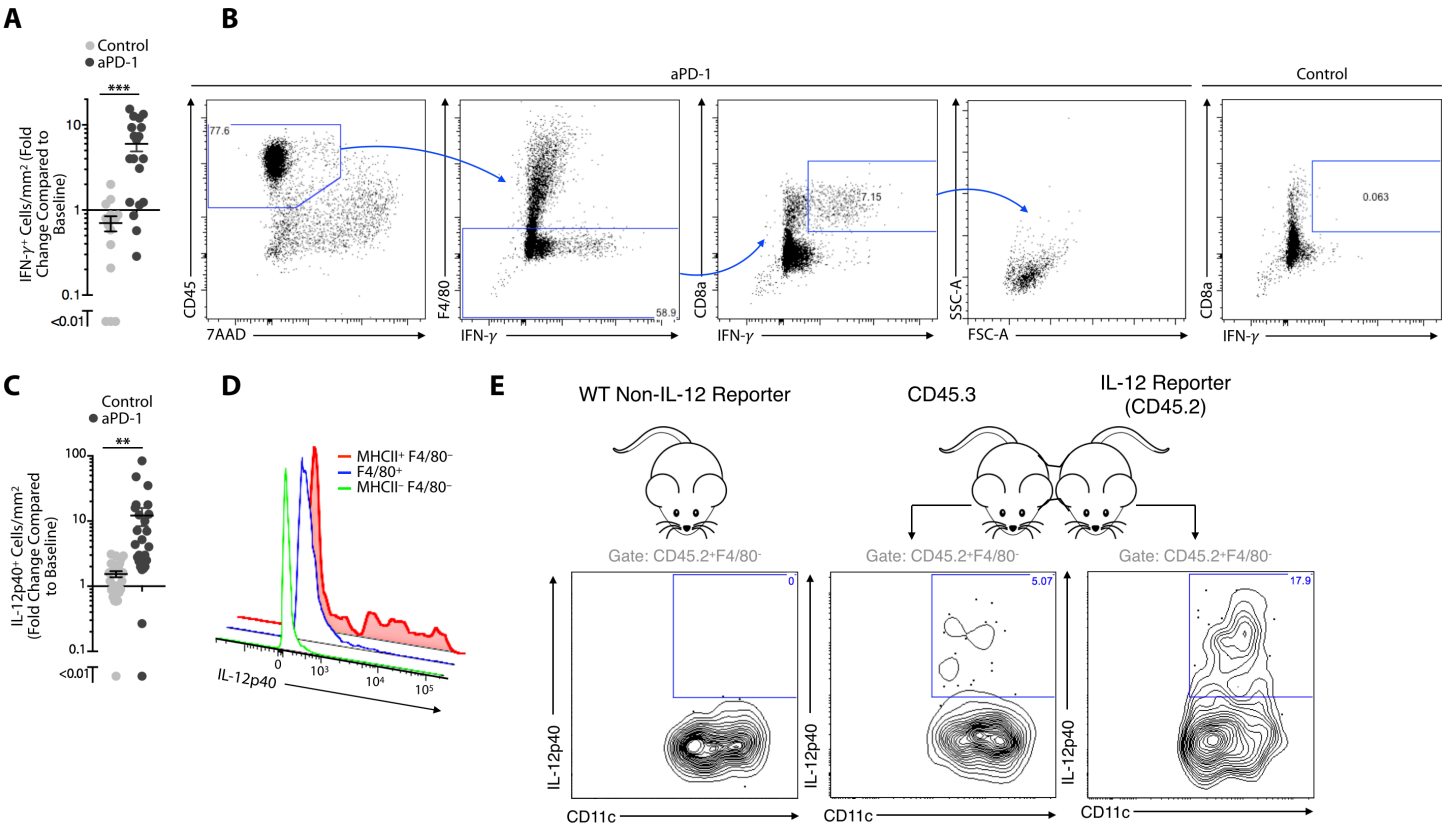

Fig. S1. Related to Figure 1. Characterization of IFN-γ^+ CD8$^+$ T Cells and IL-12p40$^+$ DCs After aPD-1 Therapy. (A) Quantification of IFN-γ signal from intravital microscopy of IFN-γ reporter mice treated or not with aPD-1 mAbs (n = 3 mice/group). Cell counts are expressed as fold change of IFN-γ^+ cells/mm^2 from pre-treatment baseline. **(B)** Flow cytometry of aPD-1-treated MC38 tumors from IFN-γ reporter mice shows IFN-γ expression by CD8α$^+$ cells. Gating strategy for IFN-γ^+ cells is shown for an aPD-1 treated sample. **(C)** IL-12p40$^+$ cells per mm^2 were quantified using intravital microscopy of MC38 tumors in IL-12p40 reporter mice treated with and without aPD-1 treatment. Values were calculated as a fold change from pre-treatment baseline (n = 5 mice/group). IL-12 and IL-23 share the p40 subunit but have contrasting roles in cancer immunity, with IL-12 as antitumor and IL-23 as pro-tumor (Yan et al., 2018). Our data indicate responses due to IL-12 biological activity considering the lack of detectable IL-23 production in this experimental setting (Figure S2A) and association of IL-12p40 with an anti-tumor response. **(D)** IL-12p40 reporter mice bearing MC38 tumors were treated with aPD-1 and tumors were harvested 3 days after treatment. Single cell suspensions of the tumors were prepared and stained for flow cytometry. Shown are the following subsets cells (pre-gated on CD45$^+$): MHCII$^+$ F4/80$^-$ (red), F4/80$^+$ (blue) and MHCII$^-$ F4/80$^-$ (green). **(E)** Congenic CD45.3 and IL-12p40 reporter mice were parabiosed and implanted with MC38 tumors. Mice were then treated with aPD-1 and tumors were isolated for flow cytometry analysis of IL-12-producing cells. Data are representative of 3 parabiotic mouse pairings. ** p-value < 0.01, Error bar values represent SEM. *Student's* t-test two tailed.

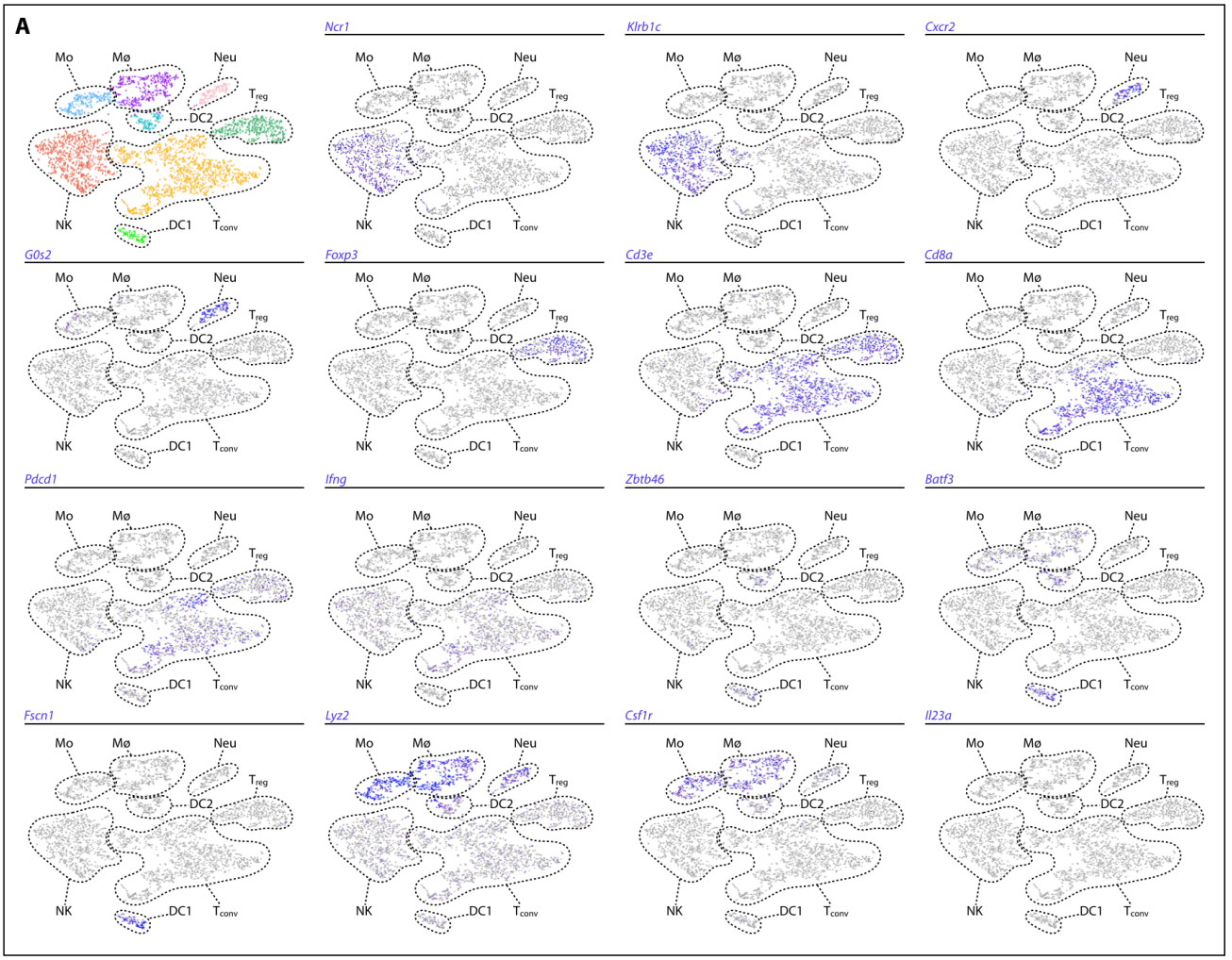
A
Mo
Mø
Neu
Treg
DC2
NK
DC1
Tconv
Ncr1
Klrb1c
Cxcr2
G0s2
Foxp3
Cd3e
Cd8a
Pdcd1
Ifng
Zbtb46
Batf3
Fscn1
Lyz2
Csf1r
Il23a

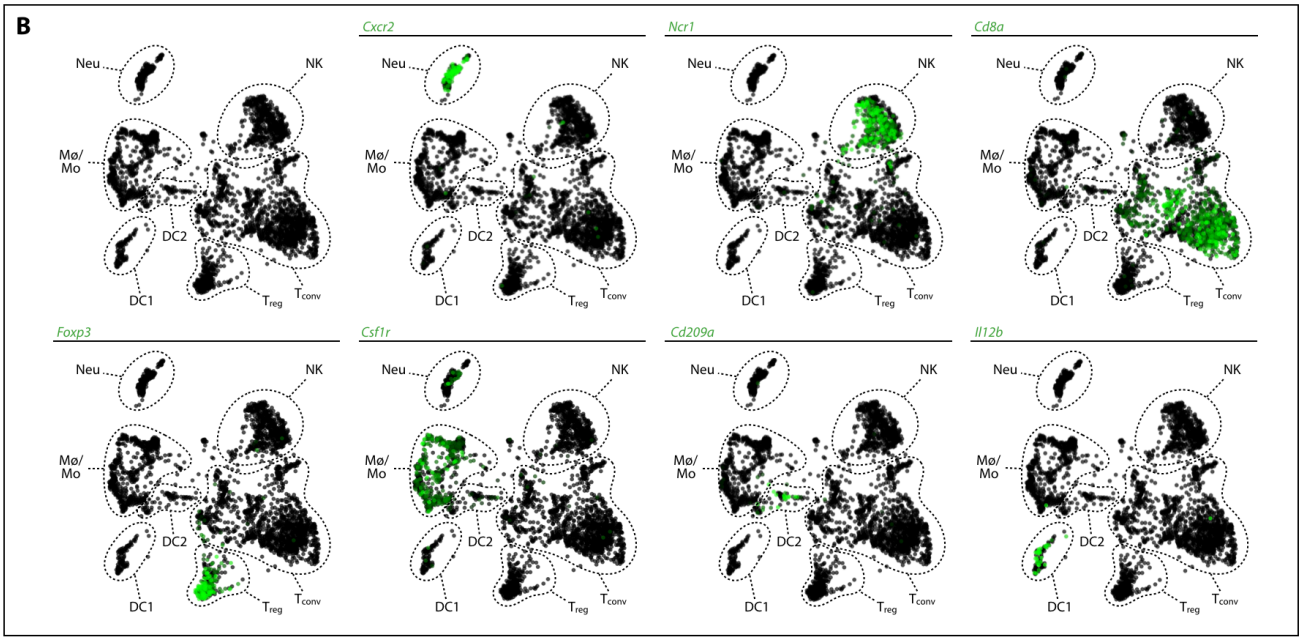
B
Neu
NK
Mø/
Mo
DC2
DC1
Treg
Tconv
Cxcr2
Ncr1
Cd8a
Foxp3
Csf1r
Cd209a
Il12b

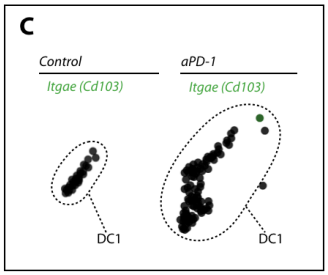
C
Control
aPD-1
Itgae (Cd103)
Itgae (Cd103)
DC1
DC1

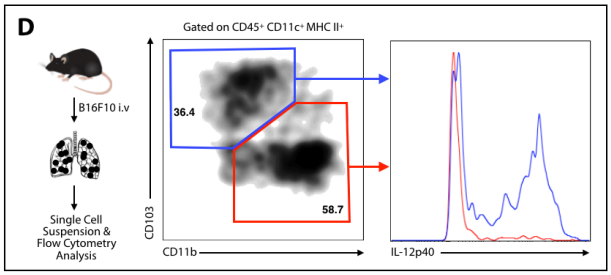
D
Gated on CD45+ CD11c+ MHC II+
B16F10 i.v
Single Cell Suspension & Flow Cytometry Analysis
36.4
58.7
CD103
CD11b
IL-12p40

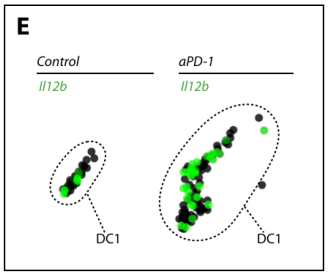
E
Control
aPD-1
Il12b
Il12b
DC1
DC1

Fig. S2. Related to Figure 2. Characterization of scRNA Sequencing of MC38 Tumor Immune Infiltrates. **(A)** t-stochastic neighbor embedding (t-SNE) feature plots are clustered according to cell lineage defining factors, and assigned to immune cell types. Examples of defining factors are enumerated, and correspond to NK populations, *Ncr1* and *Klrb1c*; Neutrophil populations, *Cxcr2* and *G0s2*; T regulatory cells, *Foxp3*; T conventional cells, *Cd3e*, *Cd8a*, *Pdcd1* and *Ifng*; Dendritic Cells, *Zbtb46*, *Batf3* and *Fscn1*, and Monocytes/ Macrophages, *Lyz2* and *Csf1r*. *Il23a* is shown as control. DC, dendritic cell; Mø, macrophage; Mo, monocyte; Neu, neutrophil; NK, natural killer cell; Tconv, conventional T cell; Treg, regulatory T cell. **(B)** SPRING plots of selected cluster defining transcripts. Neutrophils, *Cxcr2;* NK cells, *Ncr1;* $CD8^+$ T cells, *Cd8a;* T regulatory cells, *Foxp3*; Macrophages and monocytes, *Csf1r*; DC1, *Il12b*; DC2, *Cd209a.* Green colored dots identify cells expressing each respective factor. DC, dendritic cell; Mø, macrophage; Mo, monocyte; Neu, neutrophil; NK, natural killer cell; Tconv, conventional T cell; Treg, regulatory T cell. **(C)** *Itgae (Cd103)* expression in DC1 cells identified by SPRING analysis either in control (left) or aPD-1 treated (right) animals. **(D)** IL-12p40 reporter mice were injected i.v. with B16F10 cells and lungs were processed for flow cytometry after 10 days of tumor growth. DCs were separated into $CD103^+$ $CD11b^-$ (blue) and $CD103^-$ $CD11b^+$ (red) subsets. Histograms show IL-12p40 expression in these subsets. Plots are representative of 5 mice. **(E)** Same as in (C) but for *Il12b* expression.

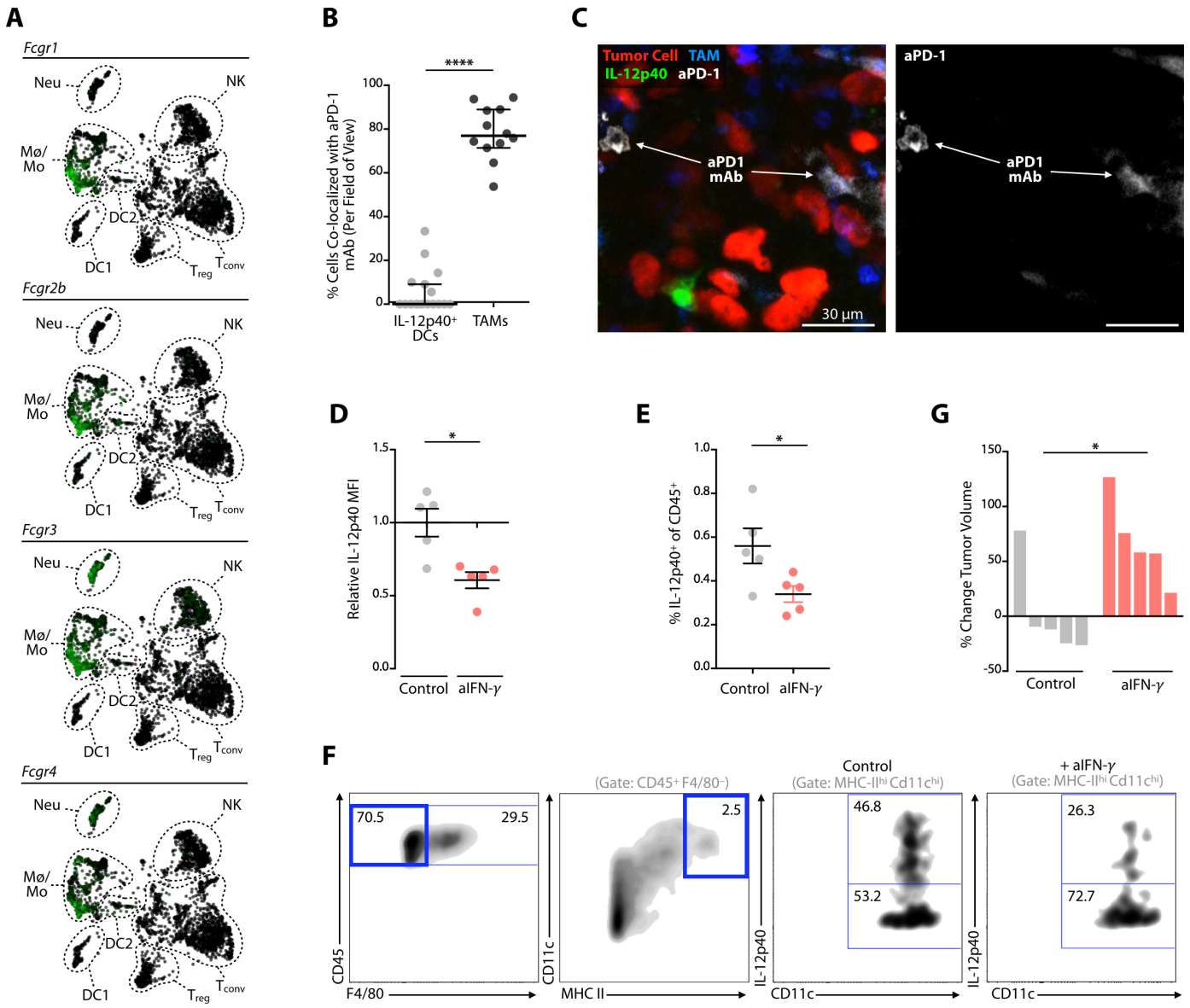

Fig. S3. Related to Figure 3. aPD-1 Induces IL-12 Production Indirectly through IFN-γ Signaling. (A) The expression pattern of selected murine Fc receptors across immune cells clustered using SPRING analysis of MC38 tumor immune infiltrates analyzed by scRNA seq. **(B)** H2B-mApple MC38 tumor-bearing IL-12p40 reporter mice were treated with AlexaFluor647-aPD-1 mAbs and analyzed by intravital imaging. The data show the percent of aPD-1 signal overlapping with IL-12p40$^+$ cells or with tumor-associated macrophages (TAMs) 24 h after aPD-1 administration. **(C)** AF647-aPD-1 mAb was administered to IL-12p40 reporter mice bearing H2B-mApple MC38 tumors and *in vivo* microscopy images above represent drug distribution within the first hour of administration. Red, MC38 tumor cells; blue, tumor associated macrophages (TAM); green, IL-12p40$^+$ cells; white, AF647-aPD-1 mAb. Scale bars represent 30 μm. **(D)** Flow cytometry measurement of IL-12p40 signal (MFI, mean fluorescent intensity) in MC38 tumors three days after aPD-1 treatment and in the presence or absence of IFN-γ neutralizing mAbs (aIFN-γ). Data normalized to baseline IL-12p40 levels from n = 5 mice per group. **(E)** Flow cytometry of IL-12$^+$ cells as a proportion of CD45$^+$ cells, using IL-12p40 reporter mice. **(F)** MC38 tumor bearing IL-12p40 reporter mice were treated with aPD-1, with or without co-administration of aIFN-γ. Tumors were collected for flow cytometry and DC populations were defined as CD45$^+$ F4/80$^-$ CD11c^{hi} MHCII^{hi}. Shown are two representative plots of control and aIFN-γ conditions from n = 5 per group, data correspond to Figure 3D. **(G)** Tumor growth of indicated animals at 3 days post aPD-1 treatment with or without aIFN-γ. Tumor size of each individual animal defines pre-treatment baseline and values reported are changes

from baseline after treatment; n = 5 mice per group. * p-value < 0.05, **** p < 0.001, Error bar values represent SEM. *Student's* two-tailed, t-test.

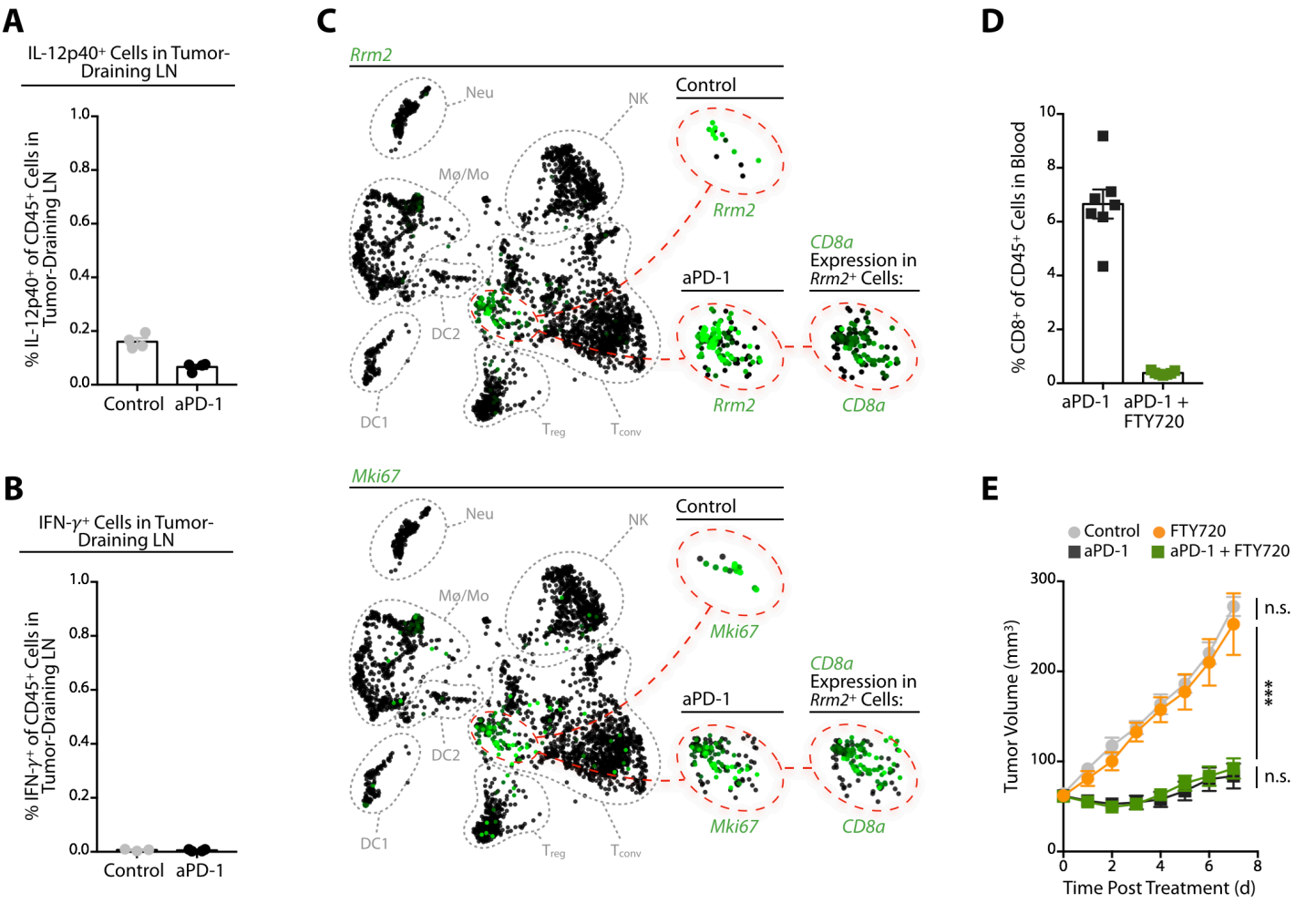

Fig. S4. Related to Figure 4. IL-12 Responses to aPD-1 mAbs Do Not Occur in the Lymph Node and aPD-1 Treatment Functions Independently of Lymphocyte Recirculation. (A) MC38 tumor-bearing IL-12 reporter mice were treated with aPD-1 or not (control), and tumor-draining lymph nodes were harvested 48 hours after treatment. Flow cytometry of IL-12$^+$ DCs is shown with control (grey) and aPD-1 (black) treatments; n = 4 mice/group. **(B)** MC38 tumor-bearing IFN-γ reporter mice were treated with aPD-1 or not (control) and tumor-draining lymph nodes were harvested 48 hours after treatment. Flow cytometry of IFN-γ^+ cells is shown with control (grey) and aPD-1 (black) treatments; n ≥ 3 mice/group. **(C)** Single cell RNA sequencing expression data of the proliferation associated genes *Rrm2* and *Mki67* within tumor immune cell populations. Comparisons are from samples treated or not with aPD-1. Cell clusters positive for either *Rrm2* or *Mki*67 are also shown to express *Cd8a*. **(D)** Blood of aPD-1-treated animals without (black) or with (green) FTY720 was analyzed by flow cytometry for circulating CD8$^+$ T cells; n ≥ 7 mice/group. **(E)** Tumor growth curves of MC38 tumor-bearing mice that received FTY720 alone (orange circle), aPD-1 alone (black square), both aPD-1 and FTY720 (green square), or that were left untreated (control, grey circle); n ≥ 6 mice/group from one experiment. n.s = not significant, *** $p < 0.001$, Error bar values represent SEM. One way ANOVA with multiple comparisons.

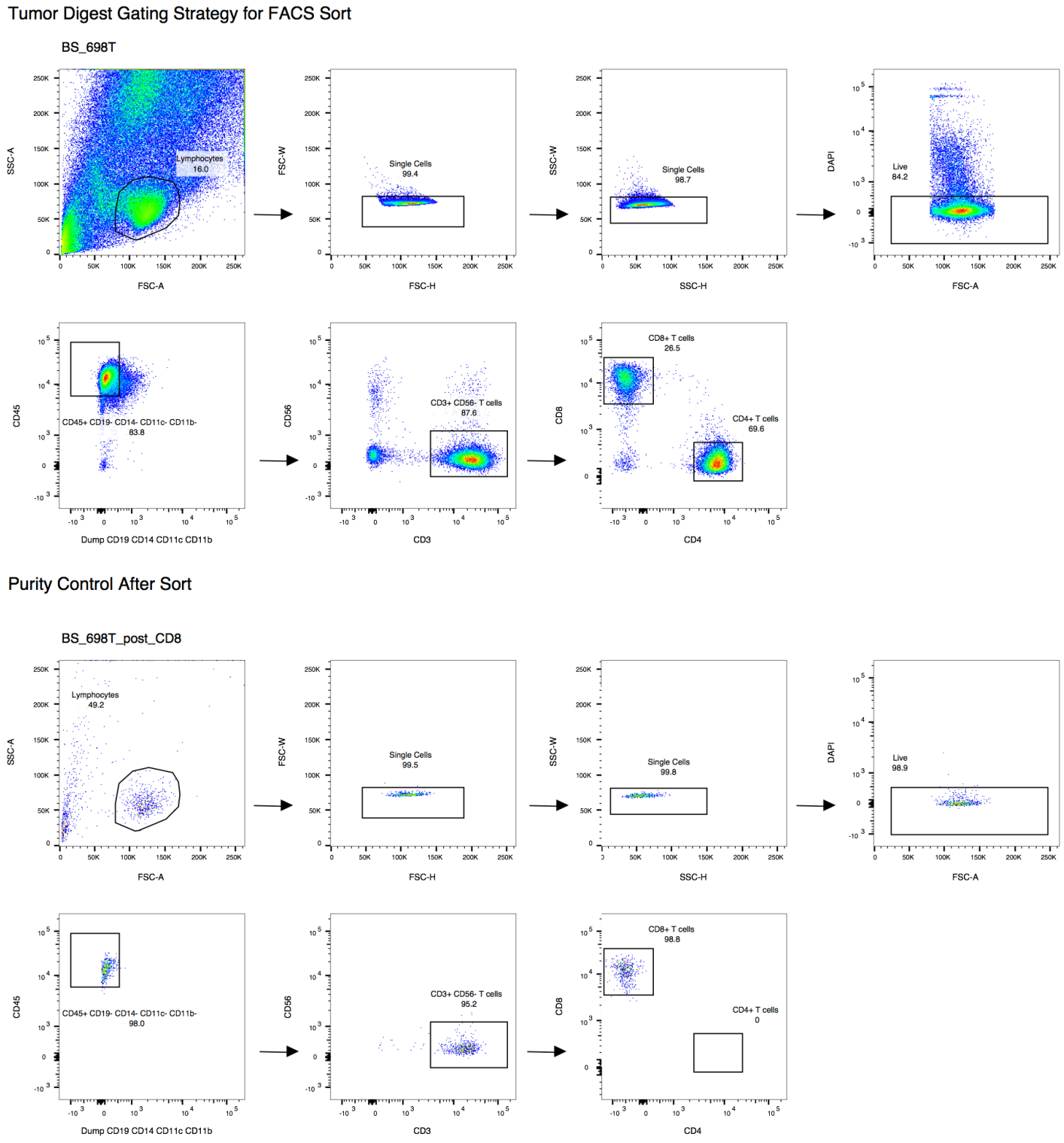

Fig. S5. Related to Figure 5. Flow Cytometry Sorting Strategy and Validation of Human Tumor Infiltrating Lymphocytes. Fresh tumor samples isolated from cancer patients were mechanically dissociated and digested into single cell suspensions, and the representative flow cytometry gating strategies for isolating $CD8^+$ T cells. Samples were re-run through the initial gating strategy to ensure sample purity.

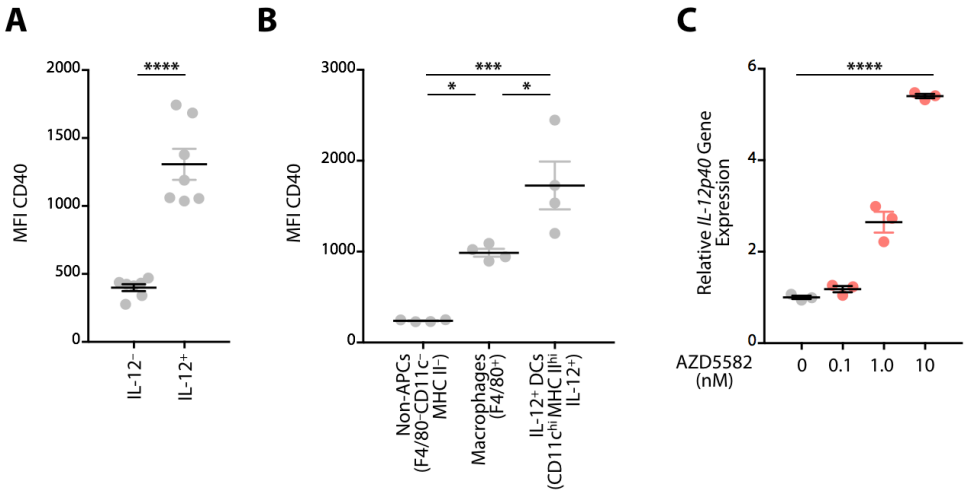

Fig. S6. Related to Figure 6. IL-12 Expressing Cells Express More CD40 and AZD5882 can Induce IL-12 Production In vitro. (A) Flow cytometry of MC38 tumors from IL-12p40-eYFP reporter mice, stained for CD40 expression; n = 7 per group. **(B)** Flow cytometry of CD40 expression from the following tumor immune cell populations: Non-Antigen Presenting Cells (non-APCs, defined as F4/80$^-$ CD11c$^-$ MHCII$^-$), macrophages (F4/80$^+$) and IL-12$^+$ DCs (CD11c^{hi} MHCII^{hi} IL-12$^+$); n = 4 per group. **(C)** Flt3L-derived bone marrow DCs were cultured in vitro with various concentrations of AZD5582 for 24 hours, and were harvested for RNA. Shown is fold change expression of IL-12p40 transcripts compared to untreated conditions (n = 3 per condition). Results are representative of at least 2 independent experiments. **** $p < 0.0001$, Error bar values represent SEM. *Student's* two tailed t-test.

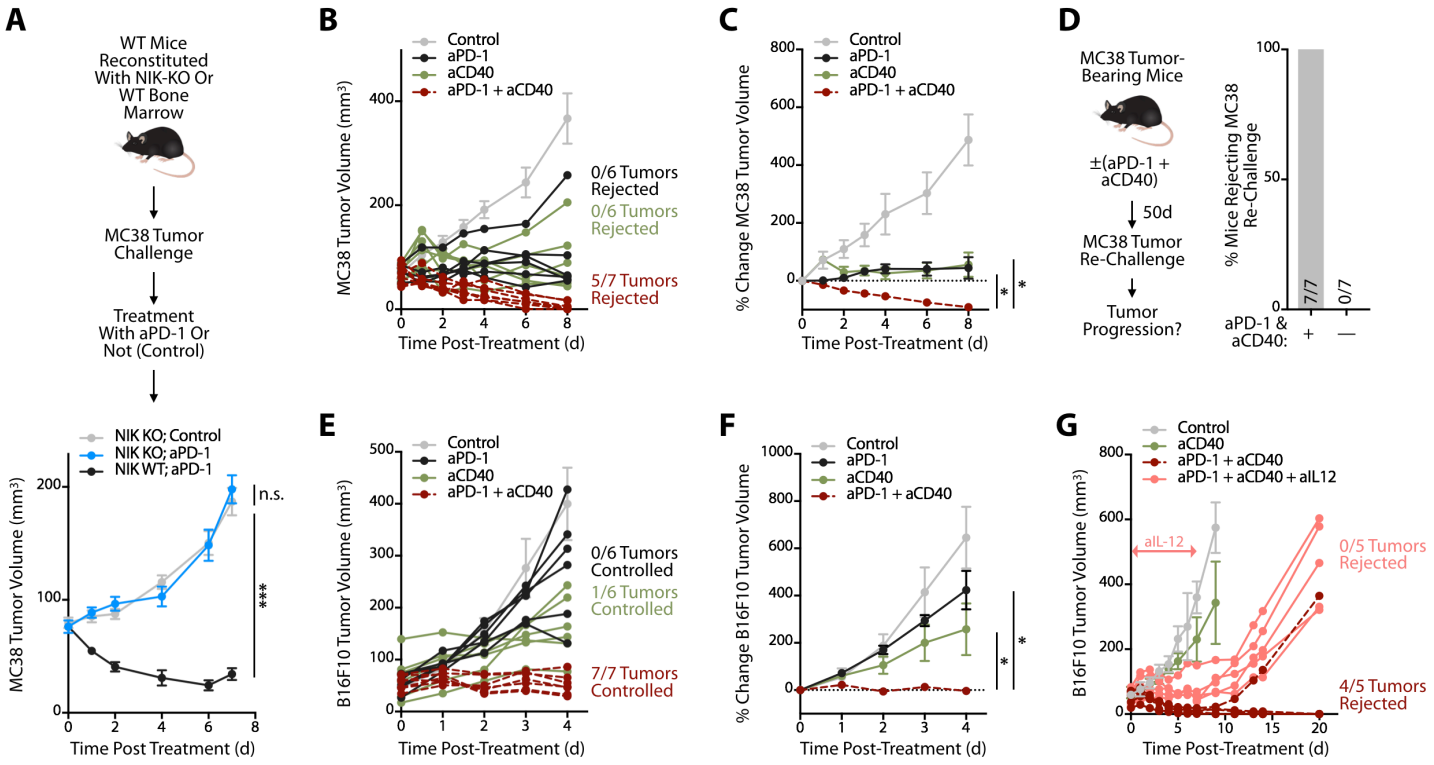

Fig. S7. Related to Figure 7. MC38 and B16 F10 Tumor Response to aPD-1 + aCD40 Combination Therapy. (A) Bone marrow chimeras reconstituted with either NIK KO or WT bone marrow were implanted with MC38 tumors and treated with aPD-1. NIK KO reconstituted mice not treated with aPD-1 were used as additional controls. The plot shown below indicates tumor progression over time in the different experimental groups (n = 5-10 mice/group). **(B, C)** MC38 tumor growth in mice that received aPD-1 mAb (black line), agonistic aCD40 mAb (green line) or aPD-1 + aCD40 combination (red line). Untreated mice were used as controls (grey line). Tumors were approximately 75 mm^3 in size at initiation of treatment (n ≥ 6 mice/group). (B) shows tumor volumes; dots for black, green and red groups represent single mice. (C) shows percent change tumor volume when compared to pre-treatment data. **(D)** MC38 bearing animals that showed a complete response to aPD-1 + aCD40 combination treatment were re-challenged with MC38 tumor cell implantation 50 days following initial tumor rejection. Naive mice that had not been exposed to MC38 were used as controls (n = 7 mice/group). Data show the percentage of mice rejecting MC38 re-challenge. **(E and F)** B16F10 tumor growth in mice that received aPD-1 mAb (black line), agonistic aCD40 mAb (green line) or aPD-1 + aCD40 combination (red line). Untreated mice were used as controls (grey line). Tumors were approximately 75 mm^3 in size at initiation of treatment (n ≥ 6 mice/group). (E) shows tumor volumes; dots for black, green and red groups represent single mice. (F) shows percent change tumor volume when compared to pre-treatment data. **(G)** B16F10 tumor volume measurements in mice that received aCD40 (green line), aPD-1 + aCD40 (red dashed line) or aPD-1 + aCD40 + aIL-12 (pink line). Untreated mice served as controls (grey circles). Dots for red and pink groups represent single mice. n ≥ 5 mice/group. Results are representative of at least 2 independent experiments. * $p < 0.05$, ** $p < 0.01$, *** $p < 0.001$, Error bar values represent SEM. One way ANOVA with multiple comparisons.